SPACE SHUTTLE PLUME/SIMULATION APPLICATION

FINAL SUMMARY REPORT

Prepared for:

NATIONAL AERONAUTICS AND SPACE ADMINISTRATION
GEORGE C. MARSHALL SPACE FLIGHT CENTER
Science and Engineering Directorate

Under Contract NAS8-32524

Prepared by:

NORTHROP SERVICES, INC.

P. O. Box 1484   Huntsville, Alabama 35807   (205) 837-0580

NSi

SPACE SHUTTLE PLUME SIMULATION APPLICATION
FINAL SUMMARY REPORT

15 May 1979

by

W. Boyle
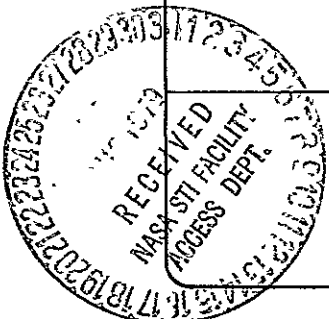B. Conine
G. Bell

Prepared for:

NATIONAL AERONAUTICS AND SPACE ADMINISTRATION
GEORGE C. MARSHALL SPACE FLIGHT CENTER
SCIENCE AND ENGINEERING DIRECTORATE

Under Contract NAS8-32524

Reviewed and Approved by:

M.A. Sloan, Jr., Manager
Technology

NORTHROP SERVICES, INC.
ENGINEERING AND TECHNOLOGY CENTER
P.O. BOX 1484
HUNTSVILLE, ALABAMA 35807
(205)837-0580

FOREWORD

This document summarizes the results of data and data analysis of two wind tunnel test programs to define the plume induced environments on the Space Shuttle vehicle. The work was performed for the NASA Marshall Space Flight Center, Huntsville, Alabama. The NASA technical monitors for this study was Mssrs. Kenneth L. Blackwell and Joseph L. Simms of the Systems Dynamics Laboratory.

TABLE OF CONTENTS

LIST OF ILLUSTRATIONS

LIST OF TABLES

GENERAL NOMENCLATURE

SYMBOL   DEFINITION

ET	Space Shuttle external tank
O	Space Shuttle Orbiter
SRB	Space Shuttle Solid Rocket Booster
SSLV	Space Shuttle Launch Vehicle
Base	Locations on the Space Shuttle where the nozzle exhaust plumes are the primary influence in determining the local pressure environment
Components	Portions of the Orbiter; wing, body flap, etc.
Elements	Primary elements of the SSLV, Orbiter, ET, SRB's
Forebody	Locations on the Space Shuttle where the nozzle exhaust plumes are the secondary influence in determining the local pressure environments

TEST NOMENCLATURE

Symbol General:	Definition
C_A	Axial force coefficient
C_{B_V}	Vertical tail bending moment coefficient
C_{B_W}	Wing-root bending-moment coefficient
C_H	Hinge moment coefficient
$C_{H_{E_I}}$	Hinge-moment coefficient for inboard elevon.
$C_{H_{E_O}}$	Hinge-moment coefficient for outboard elevon.
C_ℓ	Rolling moment coefficient
C_M	Pitching moment coefficient
C_N	Normal force coefficient
C_{N_W}	Wing normal-force coefficient
C_{T_V}	Vertical tail torsion moment coefficient
C_{T_W}	Wing-root torsion-moment coefficient
C_Y	Side force coefficient
C_{Y_N}	Yawing moment coefficient
C_{Y_V}	Vertical tail shear force coefficient
L	Reference length, in. or ft. defined in Table 6-10
S	Reference area, ft^2 defined in Table 6-10

SUBSCRIPTS

B	Base
F	Forebody – fuselage
C_P	Determined using power on pressure coefficient
DEL	Determined using power-on minus power-off delta pressure coefficient
O	Orbiter

TEST NOMENCLATURE

ET	ET
SRB	SRB
PON	Power On
POF	Power Off

GAS DYNAMIC NOMENCLATURE

Symbol	Definition
P_i	Pressure (absolute) at model surface tap i, psia
C_{P_i}	Pressure coefficient for model surface tap i.
ΔC_{P_i}	$C_{P\,Power\,On} - C_{P\,Power\,Off}$
P_{c_j}	Chamber pressure (absolute) for nozzle j, psia
P_{e_j}	Exit pressure (absolute) for nozzle j. psia
CPR_j	Chamber-pressure ratio for nozzle j
γ_j	Ratio of specific heats for nozzle J
$P_c/P_{\infty\,ORB}$	SSME chamber to freestream pressure ratio
$P_c/P_{\infty\,SRB}$	SRB chamber to freestream pressure ratio
P_c/P_e	Chamber to exit nozzle pressure ratio
P_c/P_{wall}	Chamber to nozzle wall pressure ratio
M_j	Plume boundary Mach number at nozzle lip
M_E	Nozzle exit Mach number at nozzle wall (inviscid)
N	Exponent of ratio of specific heats and in similarity parameters
δ_j	Initial plume expansion angle

Deflections:

δ_{E_I}	Left inboard elevon setting, corrected for load deflection, deg.
δ_{E_O}	Left outboard elevon setting, corrected for load deflection, deg.
γ_{NJ}	Pitch-angle of nozzle-j axis in a plane parallel to the Orbiter plane-of-symmetry, deg.
γ_{N_j}	Pitch-angle of nozzle-j axis in a plane which yaws with the nozzle, deg.
ψ_{N_j}	Yaw-angle of nozzle-j axis in an Orbiter waterplane, deg.

Test Operations:

M	Freestream Mach number.
Re/ft	Freestream unit Reynolds number, ft^{-1}.
q	Freestream dynamic pressure, psf.
P_∞	Freestream static pressure, psia.
P_T	Freestream total pressure, psia.
T	Freestream static temperature, $^{\circ}R$.
T_T	Freestream total temperature, $^{\circ}R$.
α	Model angle-of-attack, deg.
β	Model angle-of-sideslip, deg.
$T_{T_{SRB}}$	SRB supply total temperature, $^{\circ}R$.
$T_{T_{MPS}}$	MPS supply total temperature, $^{\circ}R$.
$P_{c_{MPS}}$	MPS supply total pressure, psia.
$P_{c_{SRB}}$	SRB supply total pressure, psia.

REVISIONS			
REV SYM	DESCRIPTION	DATE	APPROVAL

Section I

INTRODUCTION

An analysis of pressure and strain-gage data from Space Shuttle wind tunnel test IA119 and IA138 was performed to define the influence on aerodynamic characteristics resulting from the main propulsion system (MPS) and solid rocket booster (SRB) plumes. Aerodynamic characteristics of each of the elements, the components and total vehicle of the Space Shuttle vehicle during ascent flight was to be considered.

Test IA119 was a transonic wind tunnel test of a 0.02 scale model of the Space Shuttle launch vehicle. The test was conducted in the 11 x 11-foot section of the NASA/AMES Research Center Unitary Plan Wind Tunnel. Pressure data were obtained over the aft portions of the space shuttle wind tunnel model in addition to wing and elevon gage data.

Test IA138 was a supersonic wind tunnel test of a 0.01-scale model of the Space Shuttle launch vehicle. The test was conducted in the 9 x 7-foot section of the NASA/AMES Research Center Unitary Plan Wind Tunnel. Pressure data were obtained over the aft portions of the space shuttle wind tunnel model. Wing and elevon gage data were also obtained.

The simulant gas used to develop the model exhaust plumes was air. A portion of the tests were devoted to testing at various power levels. Data from the power level portion was used in conjunction with prototype possibility curves to evaluate nominal power levels. The nominal power levels were used during the investigation of changes in model attitude, elevon deflections and nozzle gimbal angles on the aerodynamic characteristics. The simulation parameter used to develop nominal power levels was $[\delta_j \gamma_j^N]_{PROT} = [\delta_j \gamma_j^N]_{MODEL}$ where N varies with Mach number.

Aerodynamic loads induced by the plumes were developed for the Space Shuttle base areas and forebody areas. The base areas are, the orbiter base including nozzles, the ET base and the SRB base. The forebody includes those areas of the orbiter forward of the base. The forebody includes the body flap, the wings and elevons, and the ET and SRB areas forward of the base.

A math model of the plume induced aerodynamic characteristics designed to·match the forebody aerodynamic math model was developed for·a range of Mach numbers. The aerodynamic characteristics of the base are presented in terms of forces and moments versus attitude. The aerodynamic characteristics of the total vehicle base and forebody are presented in terms of aerodynamic coefficients for the range of Mach numbers from 0.6 to 2.5. Aerodynamic characteristics of the elements component base and vehicle forebody are presented for Mach numbers from 0.6 to 2.5. Aerodynamic characteristics are presented vs Mach numbers compatible with Mach numbers used in defining forebody aerodynamic characteristics.

Tolerance values were developed for all plume induced aerodynamic characteristics. The tolerance values were developed in terms of a math model and include simulation parameter uncertainties, model instrumentation uncertainties, model configuration uncertainties (including tunnel-model support interference uncertainties and Reynolds number effects).

The results of the above analysis and math model of the IA119 transonic data are presented in detail in reference 1. The result of the base pressure integration computer program, gage data, and plotted data are presented in the appendix to reference 1.

The results of the analysis and math model of the IA138 supersonic data are presented in reference 2. The results of the IA138 base pressure integration computer program, gage data, and plotted data are presented in the appendix to reference 2.

Brief discussions of the wind tunnel test programs, data analysis tasks and analysis procedures are presented in the following sections. Examples of the results and math models of the results are also presented.

Section II

WIND TUNNEL MODELS

The wind tunnel model used for the IA119 test was a .02 scale Space Shuttle Launch Vehicle configuration. The wind tunnel model is designated - 88 OTS Configuration 140C (modified) Jet - Plume Integrated Space Shuttle Vehicle. The wind tunnel model is essentially the same as was used for an earlier Space Shuttle plume test IA19, conducted in 1974. The major difference being that the contoured SSME flow through nozzles were used during the IA119 test and conical SSME nozzles were used during the IA19 test. The orbiter model was the 140C model configuration which generally represents the OV101 orbiter mold lines. The OV102 mold lines have significant differences in the canopy contour, the wing section near the glove-wing fairing, and the elevon contour. Details of the model configuration can be obtained from the pretest report (reference [3]).

The model was strut mounted as shown in Figure 2-1. Cold air was supplied through the strut to the SSME and SRB nozzles. An air supply strut was mounted between the ET and orbiter to supply air to the simulated SSME nozzles as shown in Figure 2-2. The SSME nozzles were contoured with an exit plane lip angle of 5 degrees. The SRB nozzles were conical with a lip angle of 27.5 degrees.

The left orbiter wing was strain-gage instrumented to obtain wing shear forces, root bending moments and torsion moments. The inboard and outboard elevons on the left wing were separately strain-gage instrumented to obtain hinge moments. The vertical tail was also strain-gage instrumented to obtain shear, bending moments, and torsion moments. The right orbiter wing and elevons were pressure instrumented. All base, nozzle, and portions of each element forebody area were pressure instrumented.

The flow through MPS nozzles and SRB nozzles were capable of being set at various gimbal-angle positions and several gimbal patterns were investigated. The inboard and outboard elevons were also capable of being set at various deflection angles and data were obtained for a series of elevon deflection combinations.

The wind tunnel model used for the IA138 test was a 0.01 scale space shuttle launch vehicle configuration. The wind tunnel model is designated - 75 OTS Configuration 140C (modified) Jet - Plume Integrated Space Shuttle Vehicle. The orbiter model was the 140C model configuration which generally represents the OV101 orbiter mold lines. The OV102 mold lines have significant differences in the canopy contour, the wing section near the glove-wing fairing, and the elevon contour. Details of the model configuration can be obtained from the pretest report (reference 4).

The model was strut mounted similar to the IA119 model as shown in Figure 2-1. Cold air was supplied through the strut to the SSME and SRB nozzles. An air supply strut was mounted between the ET and orbiter to supply air to the simulated SSME nozzles as shown in Figure 2-2. The SSME nozzles were conical with an exit plane lip angle of 11.0 degrees. The SRB nozzles were conical with a lip angle of 27.5 degrees.

A partial right orbiter wing was strain-gage instrumented to obtain wing shear forces, root bending moments and torsion moments. The inboard and out-board elevons on the left wing were also separately strain-gage instrumented to obtain hinge moments. All base, nozzle, and portions of each element fore-body were pressure instrumented.

TUNNEL CEILING

NOTE: ALL DIMENSIONS ARE IN INCHES

VERTICAL STRUT

HIGH PRESSURE
AIR OUTLETS
2.5 INCH FEMALE PIPE

T.S.	T.S.
357.625	342.5
R.H.	L.H.
SIDE	SIDE

T.S. = 249.78

40.0

25.0

16.5

CENTER OF ROTATION
TUNNEL STATION   T.S. = 182.0
MODEL STATION X_T = 47.50

AMES
"GREEN WEENIE"
EXTENSION

CENTER OF ROTATION
TUNNEL STATION
T.S. = 304.75

2-3

TUNNEL FLOOR

TR-1964
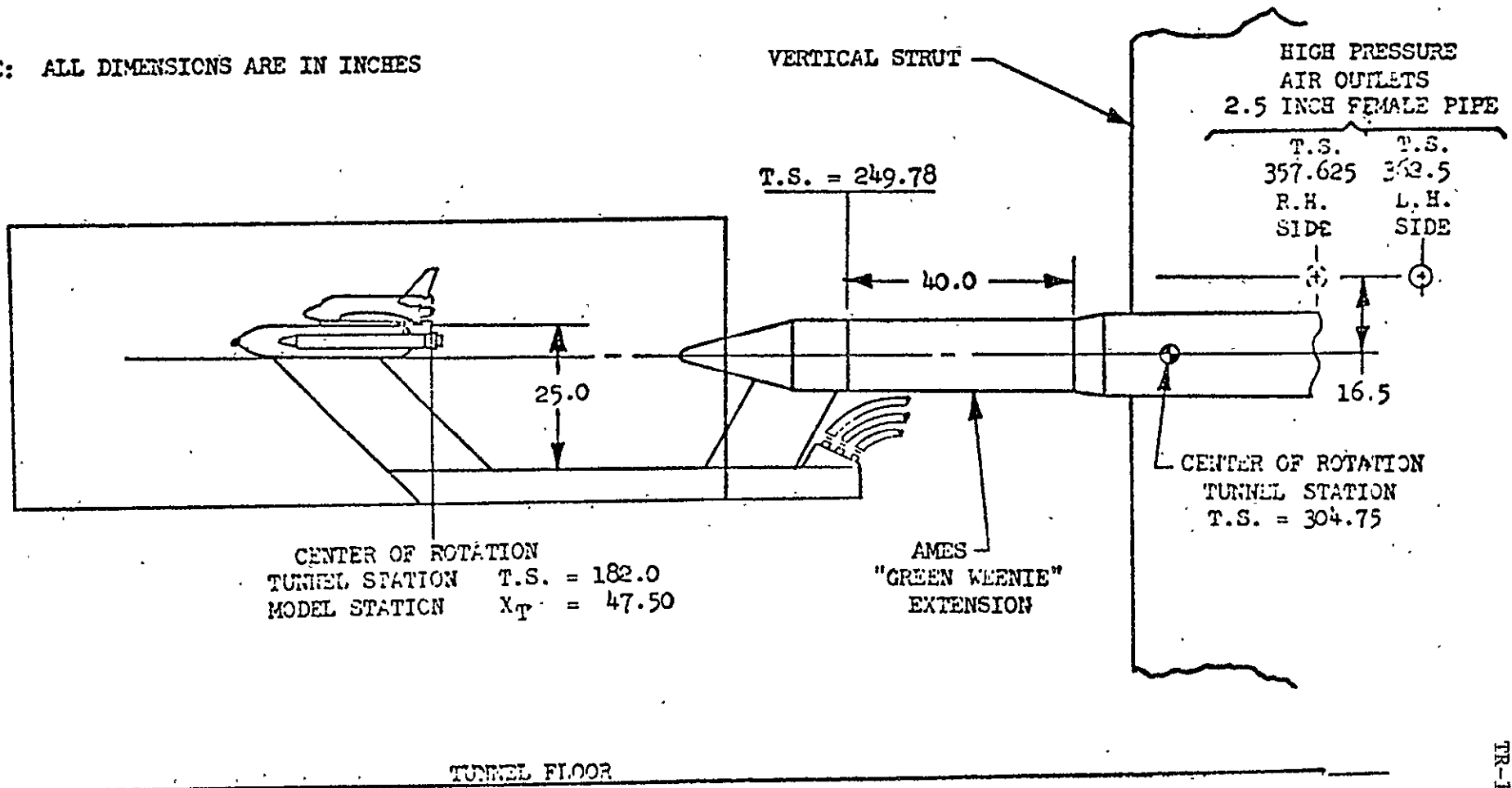
Figure 2-1. IA119 MODEL INSTALLATION

SSME NOZZLE AIR
SUPPLY STRUT

SRB NOZZLE AIR
SUPPLY STRUT

SSME FLOW THROUGH
NOZZLES

SRB FLOW THROUGH
NOZZLE

MAIN STRUT AND
AIR SUPPLY
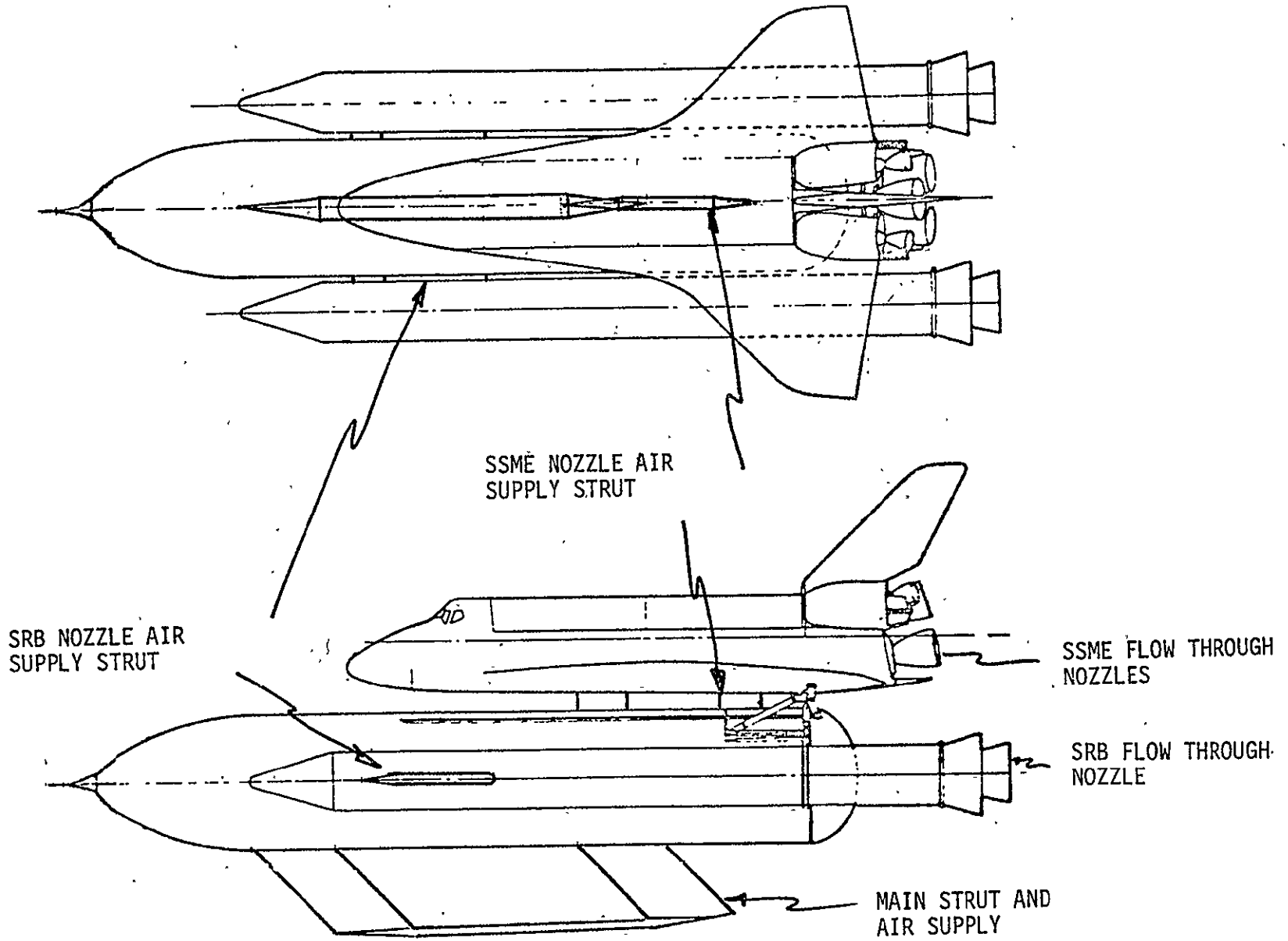
Figure 2-2.   FLOW THROUGH NOZZLE AIR SUPPLY STRUTS — IA119 MODEL

Section III

TEST CONDITIONS

The IA119 and the IA138 wind tunnel test program was essentially conducted in two parts. Part one was a power variation test at zero attitude, where chamber pressure of the MPS and SRB model nozzles was varied. Part two was a test program at a nominal power level that included various·elevon deflections, nozzle gimbal patterns, and attitudes.

Base pressure data, from the power variation tests (Part 1), was evaluated at the test site along with prototype plume characteristics to evaluate the nominal model nozzle plume characteristics and model chamber pressures. (See Section V for plume simulation discussion). These tests were conducted at zero angle of attack and zero angle of sideslip. Tests were conducted for a series of Mach numbers from 0.6 to 2.5.

Part 2 of the test programs consisted of testing the model using the nominal power levels developed in Parts 1 over a range of attitudes and configurations (elevon deflections, gimbal angles, etc.). Data were obtained at nominal angles of attack of -8, -6, -4, 0, and +4 degrees.—The angles of sideslip were nominally 0, and ± 6 or ± 4 degrees.

Tests were conducted at various elevon deflections corresponding to Schedule 6 and probable variations about schedule 6. Schedule 6 elevon deflections are presented in Figure 3-1. Plots of the various inboard and outboard elevon deflection angles evaluated during the test along with the nominal schedule 6 value are presented in Figures 3-2 through 3-10. The elevon deflection closest to schedule 6 that was used to develop the plume induced aerodynamic data base is shown in each figure.

— — — UNCERTAINTY BAND
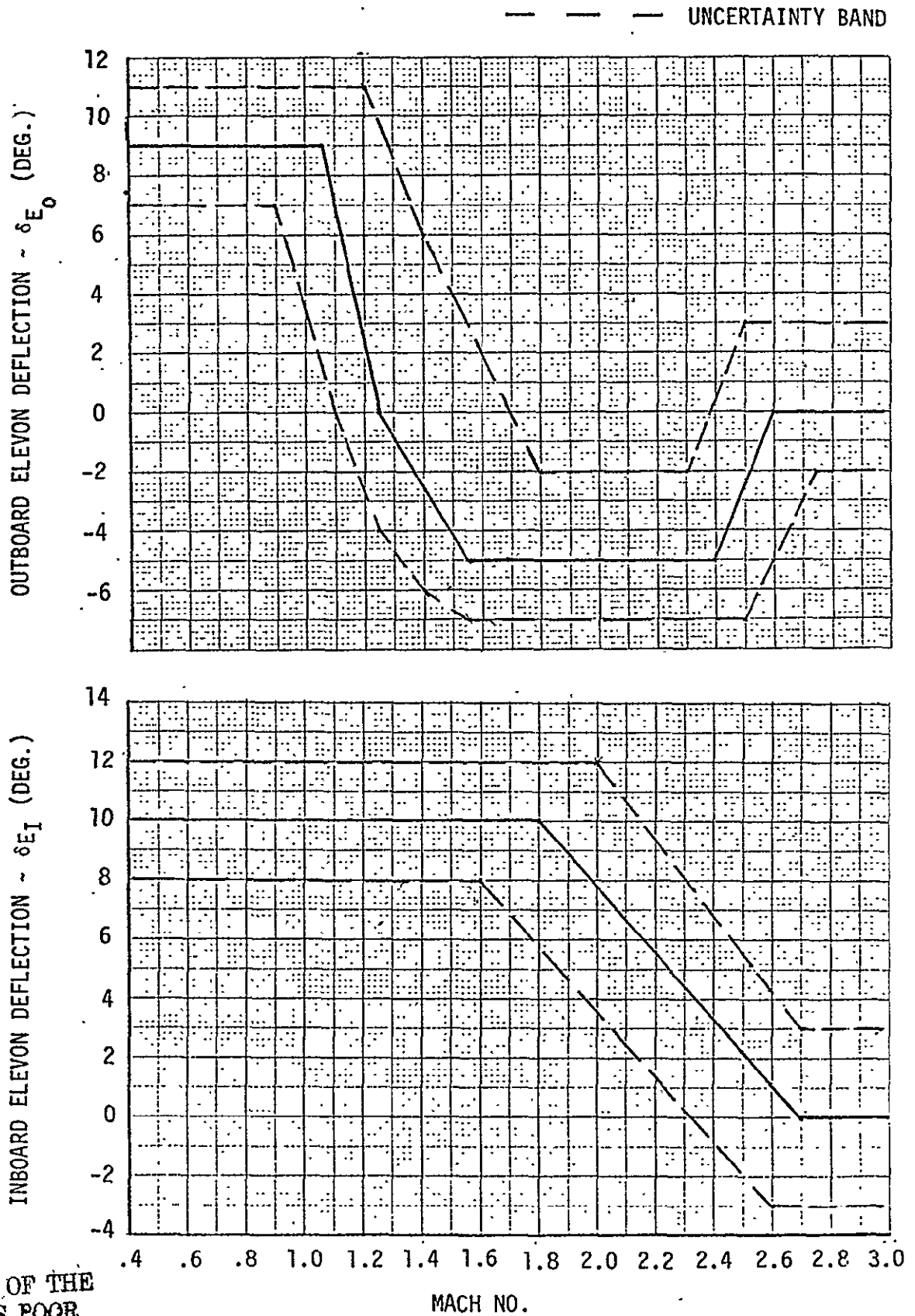
Figure 3-1. SCHEDULE 6 ELEVON DEFLECTIONS
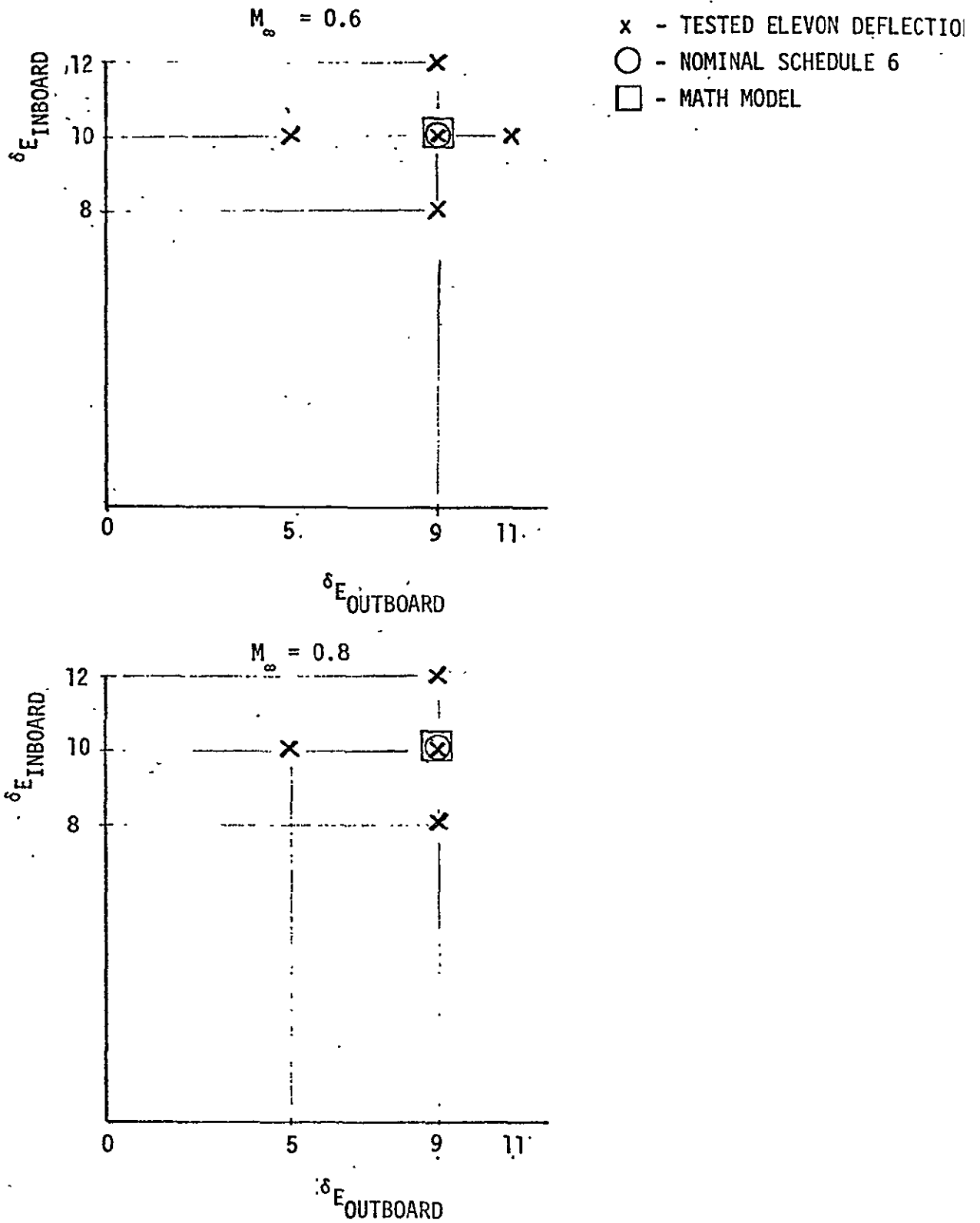
Figure 3-2.   ELEVON SCHEDULE

$M_\infty = 0.9$

x   – TESTED ELEVON DEFLECTION
○ – NOMINAL SCHEDULE 6
□ – MATH MODEL

$\delta E_{INBOARD}$

$\delta E_{OUTBOARD}$

$M_\infty = 0.95$

$\delta E_{INBOARD}$

$\delta E_{OUTBOARD}$
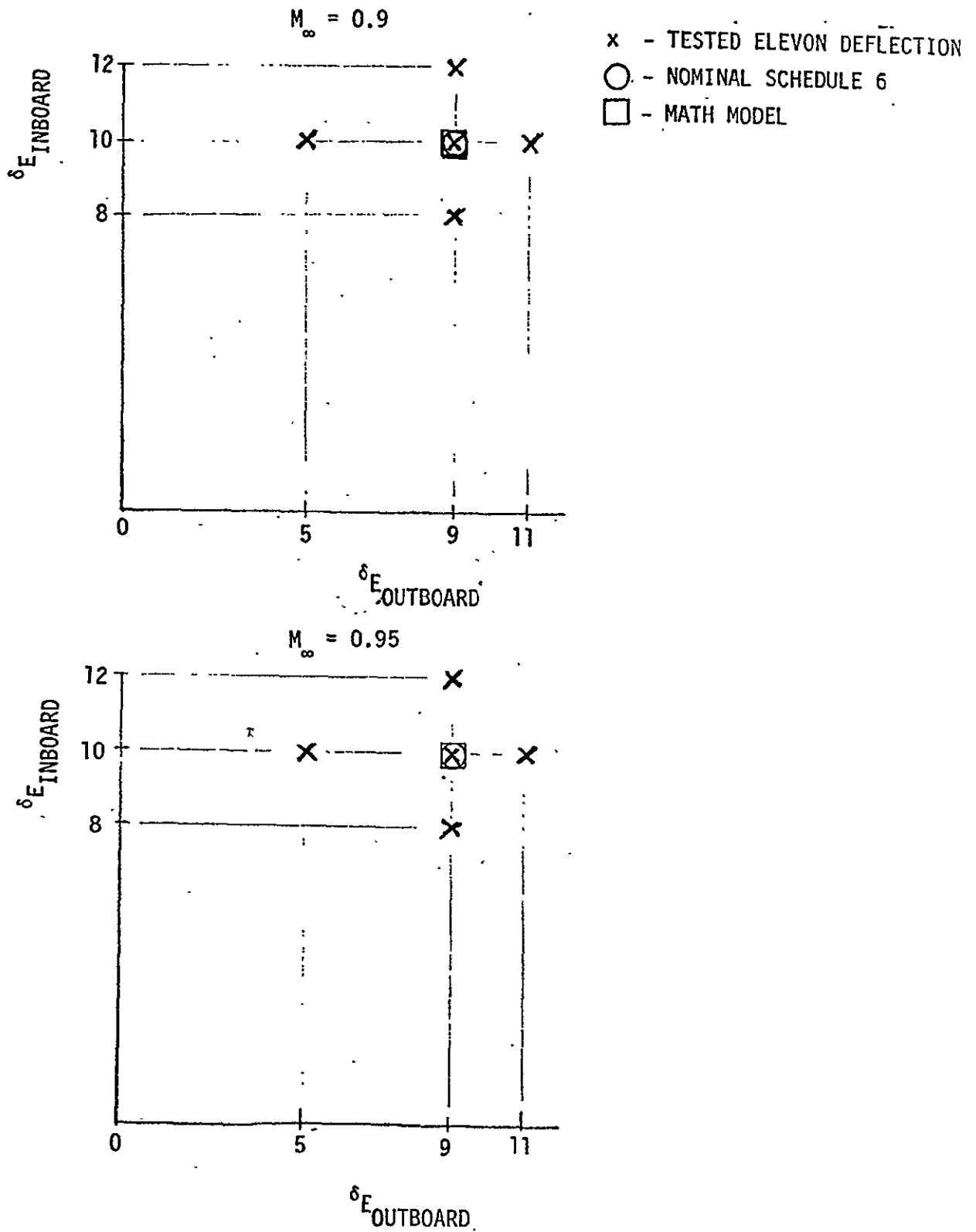
Figure 3-3.   ELEVON SCHEDULE

M = 1.05

.x – TESTED ELEVON DEFLECTION
O – NOMINAL SCHEDULE 6
□ – MATH MODEL ·

M = 1.1
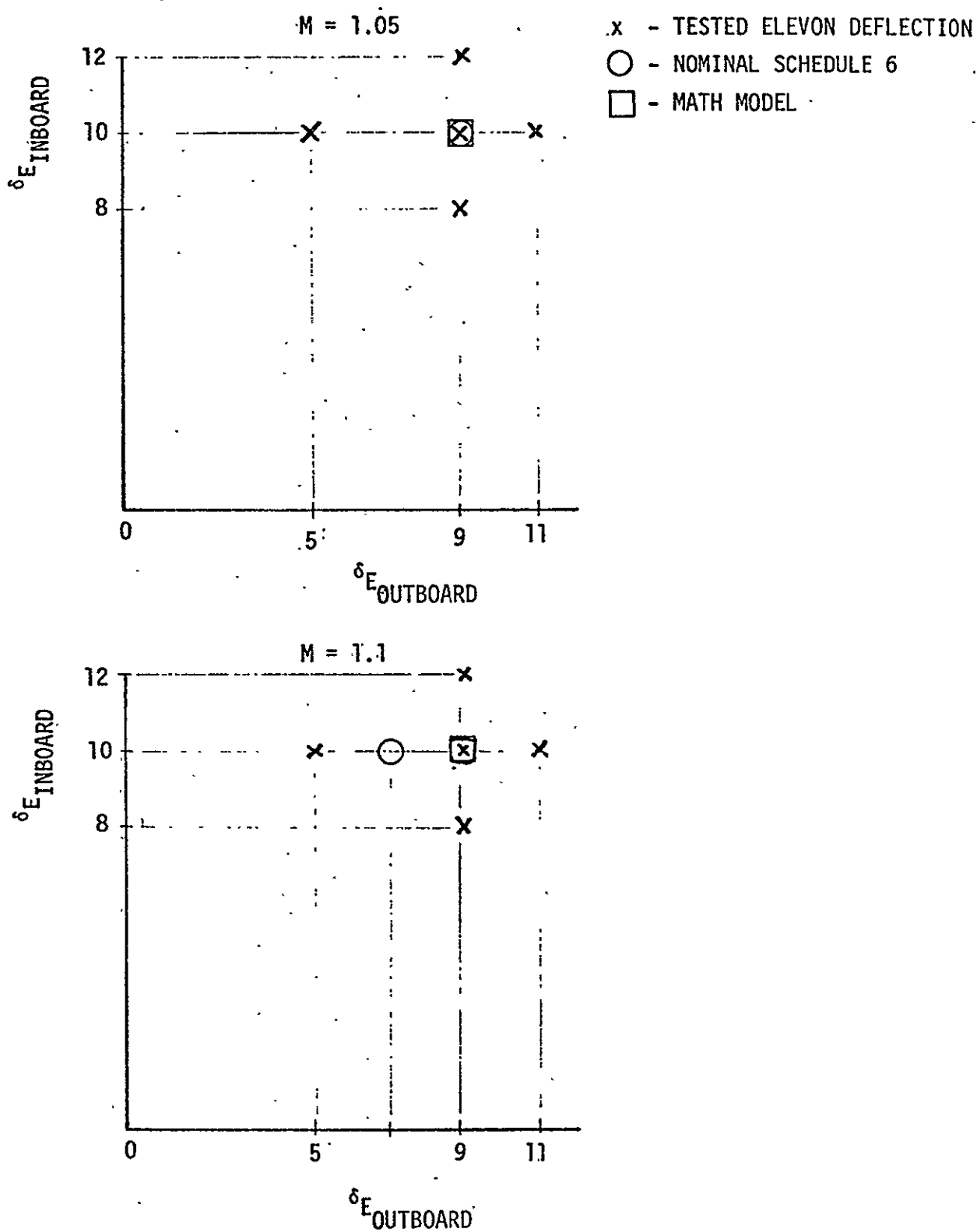
Figure 3-4.   ELEVON SCHEDULE

x — TESTED ELEVON DEFLECTION
O — NOMINAL SCHEDULE 6
□ — MATH MODEL

M = 1.15

M = 1.25
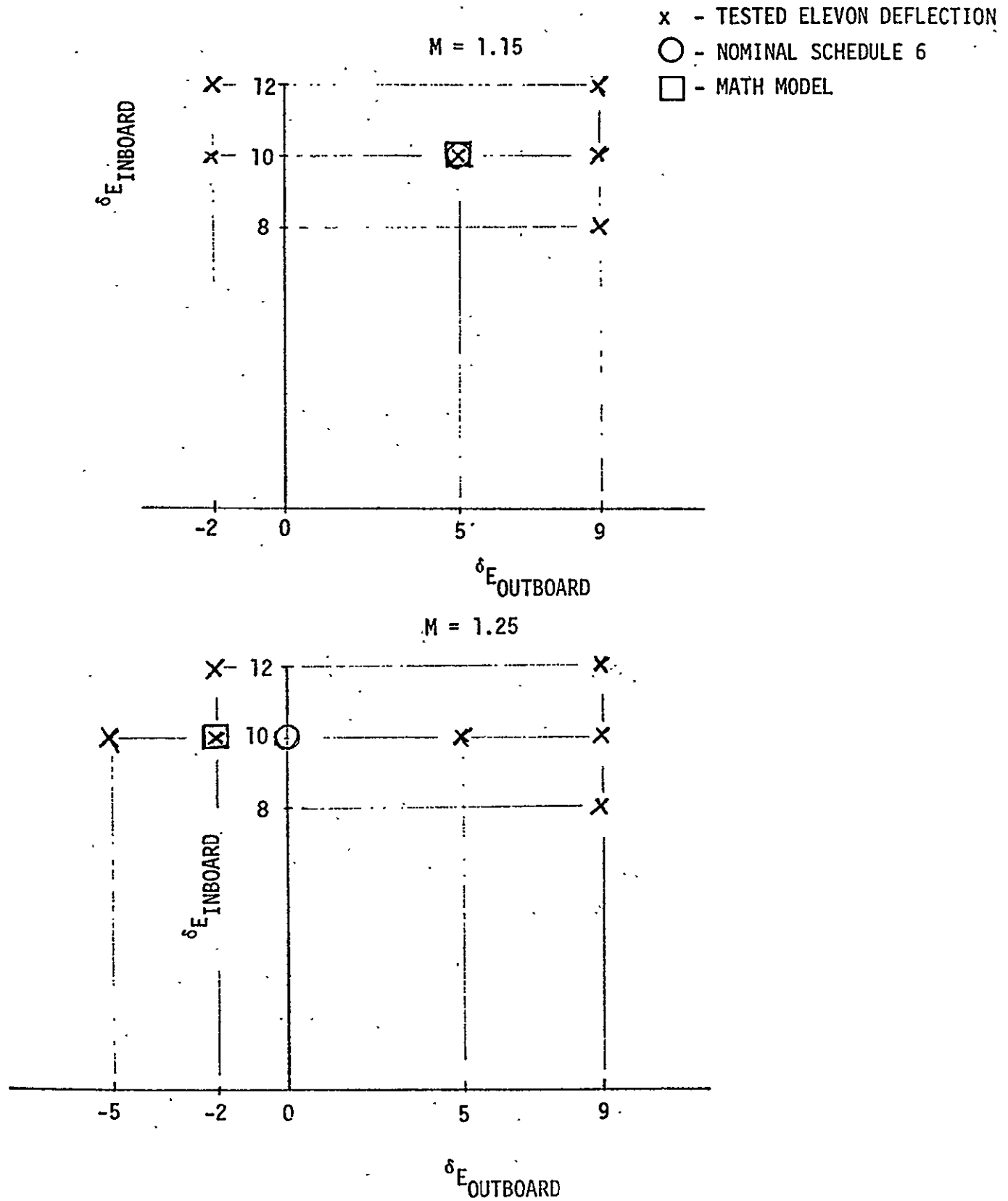
Figure 3-5.   ELEVON SCHEDULE

x - TESTED ELEVON DEFLECTION
O - NOMINAL SCHEDULE 6
□ - MATH MODEL

$M_\infty = 1.4$
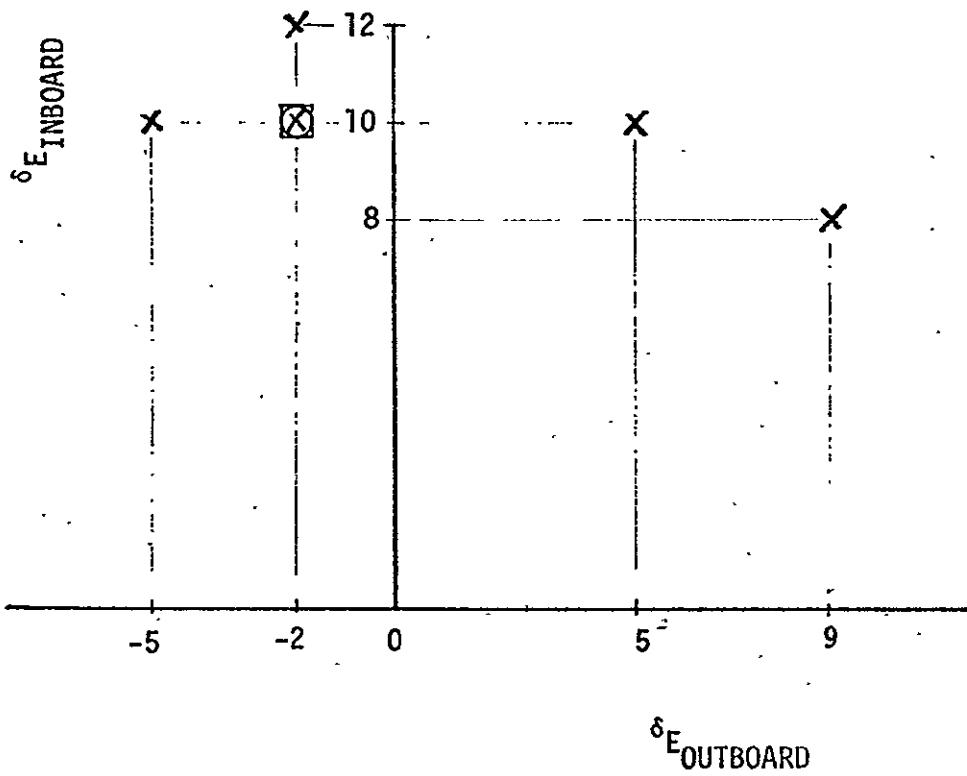
Figure 3-6.   ELEVON SCHEDULE

X — TESTED ELEVON DEFLECTION

⊙ — SCHEDULE 6

□ — MATH MODEL
10,-2
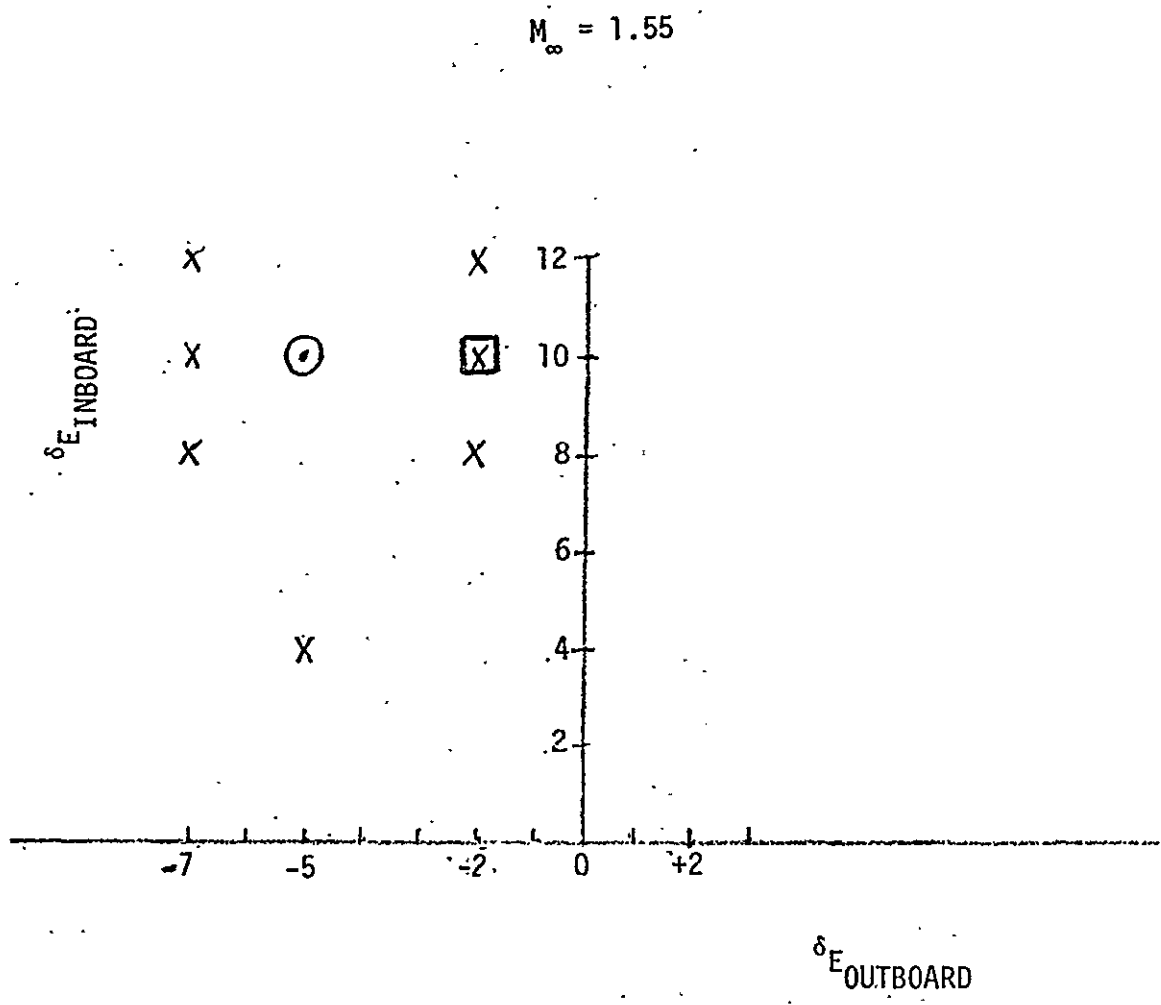
$M_\infty = 1.55$

Figure 3-7. ELEVON DEFLECTION MATRIX ($M_\infty = 1.55$)

X — TESTED ELEVON DEFLECTION
⊙— SCHEDULE 6
□ — MATH MODEL
    10,-5

$M_\infty = 1.8$
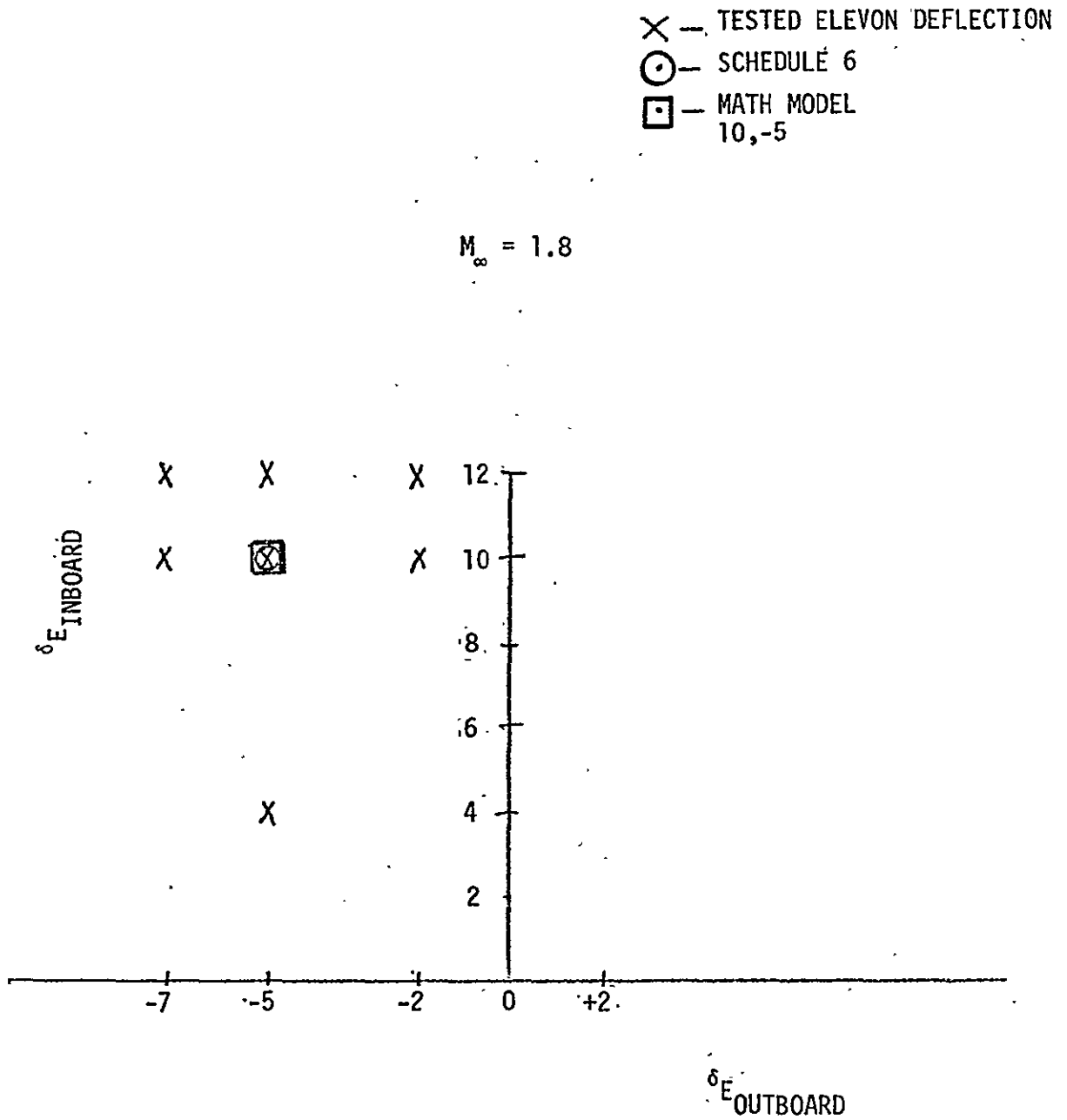
Figure 3-8. ELEVON DEFLECTION MATRIX ($M_\infty = 1.80$)

X — TESTED ELEVON DEFLECTION
⊙ — SCHEDULE 6
⊡ — MATH MODEL
4,-5

$M_\infty = 2.2$
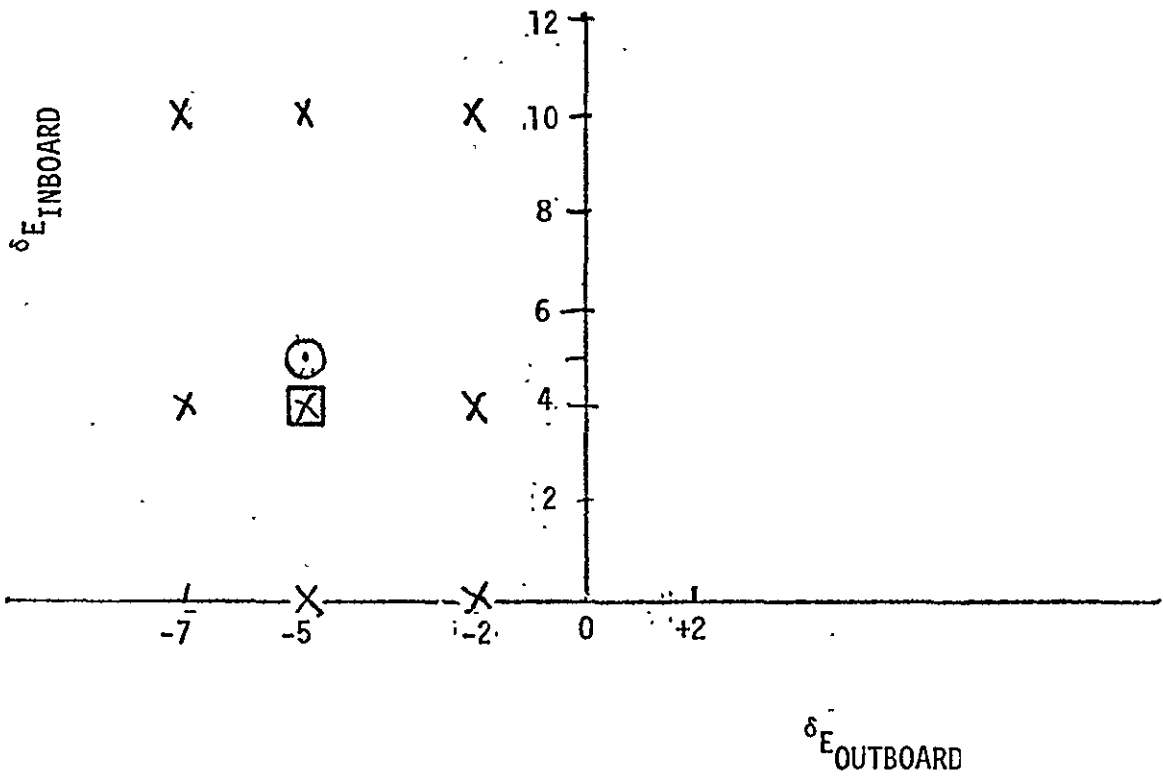
Figure 3-9.   ELEVON DEFLECTION MATRIX ($M_\infty = 2.20$)

X— TESTED ELEVON DEFLECTION

⊙— SCHEDULE 6

▣— MATH MODEL
0,-2

$M_\infty = 2.5$
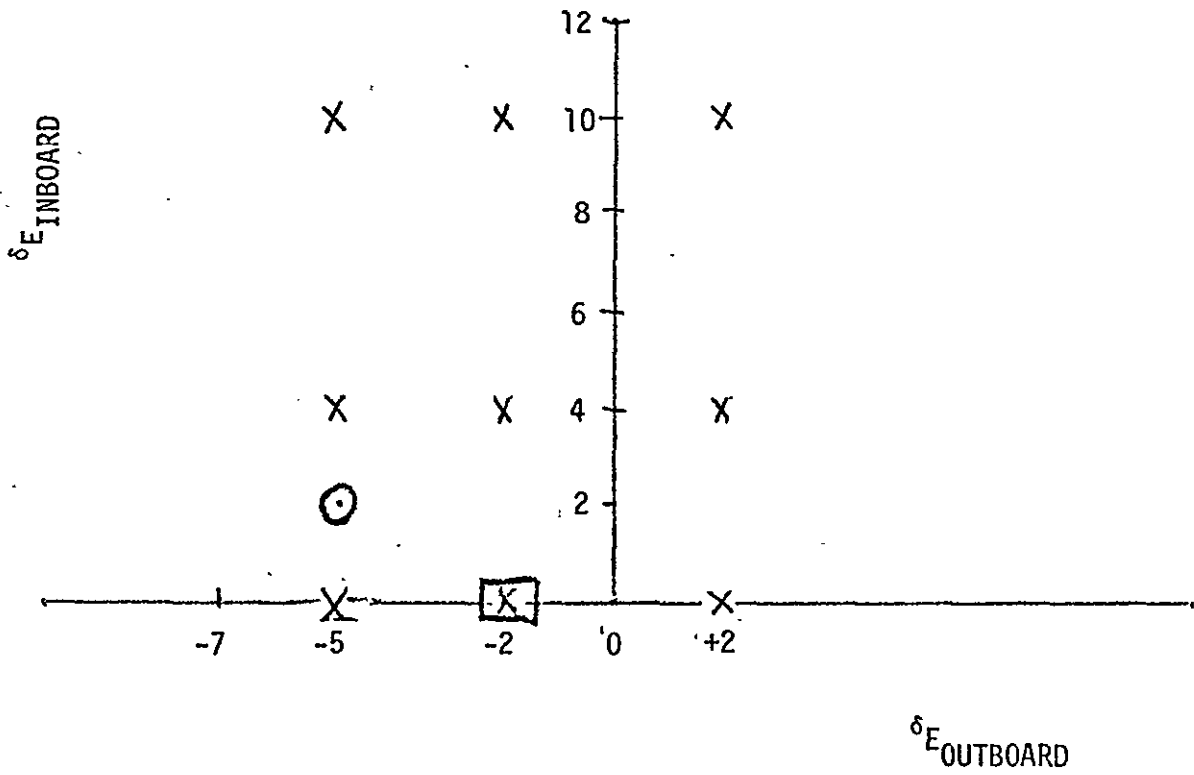
Figure 3-10. ELEVON DEFLECTION MATRIX ($M_\infty = 2.50$)

Section IV

WIND TUNNEL MODEL NOZZLE CALIBRATION ANALYSIS

An analysis of the model nozzle calibration data was performed to determine nozzle flow characteristics for the evaluation of model power levels. A range of model power levels were required for the power level variation portion of the test. Model nozzle wall pressures and exit plane pressures were plotted and compared with MOC results to evaluate the nozzle flow characteristics and to evaluate chamber to exit pressure ratios. The chamber to exit pressure ratios were required to evaluate the model plume characteristics.

Initially it was anticipated that several model nozzle configurations would be used during the IA119 test program and thus a considerable amount of calibration data were evaluated. The IA119 test program ultimately used only the 2% contoured SSME nozzle configuration and the 2% conical SRB nozzle configuration. The nozzle calibration tests were conducted for the IA19 Space Shuttle plume test (reference 5). This test (IA19) used essentially the same model hardware as the IA119 test. The IA138 test program used a 1% conical SSME nozzle configuration and a 1% conical SRB nozzle configuration.

Summary. IA119 model nozzle performance data are presented in Figures 4-1 and 4-2 for the SSME model nozzles and the SRB model nozzles respectively. The average chamber to exit plane pressure used for the model SSME nozzle was 49.5. The average chamber to exit plane pressure used for the SRB nozzle was 66.0. These values were used to develop pretest pressure ratios for each Mach number.

Summary IA138 nozzle performance data are presented in Figures 4-3 and 4-4 for the SSME nozzles and the SRB nozzles respectively. The post-test SRB nozzle performance was slightly different from the pre test nozzle performance developed from the nozzle calibration data.

TEST 7503

2% CONTOURED SSME

⊙ – NOZZLE 100 #1 TOP
◻ – NOZZLE 200 #2 LEFT
△ – NOZZLE 300 #3 RIGHT

POST TEST ≈55 · NOZZLE #2

49.5 At

P_c/P_θ

70
60
50
40
30
20

400

800

1200

$P_c \sim PSI$

Figure 4-1.   SSME NOZZLE CHAMBER TO EXIT PRESSURE RATIO — IA119

Figure 4-2. SRB NOZZLE CHAMBER TO EXIT PRESSURE RATIO — IA119
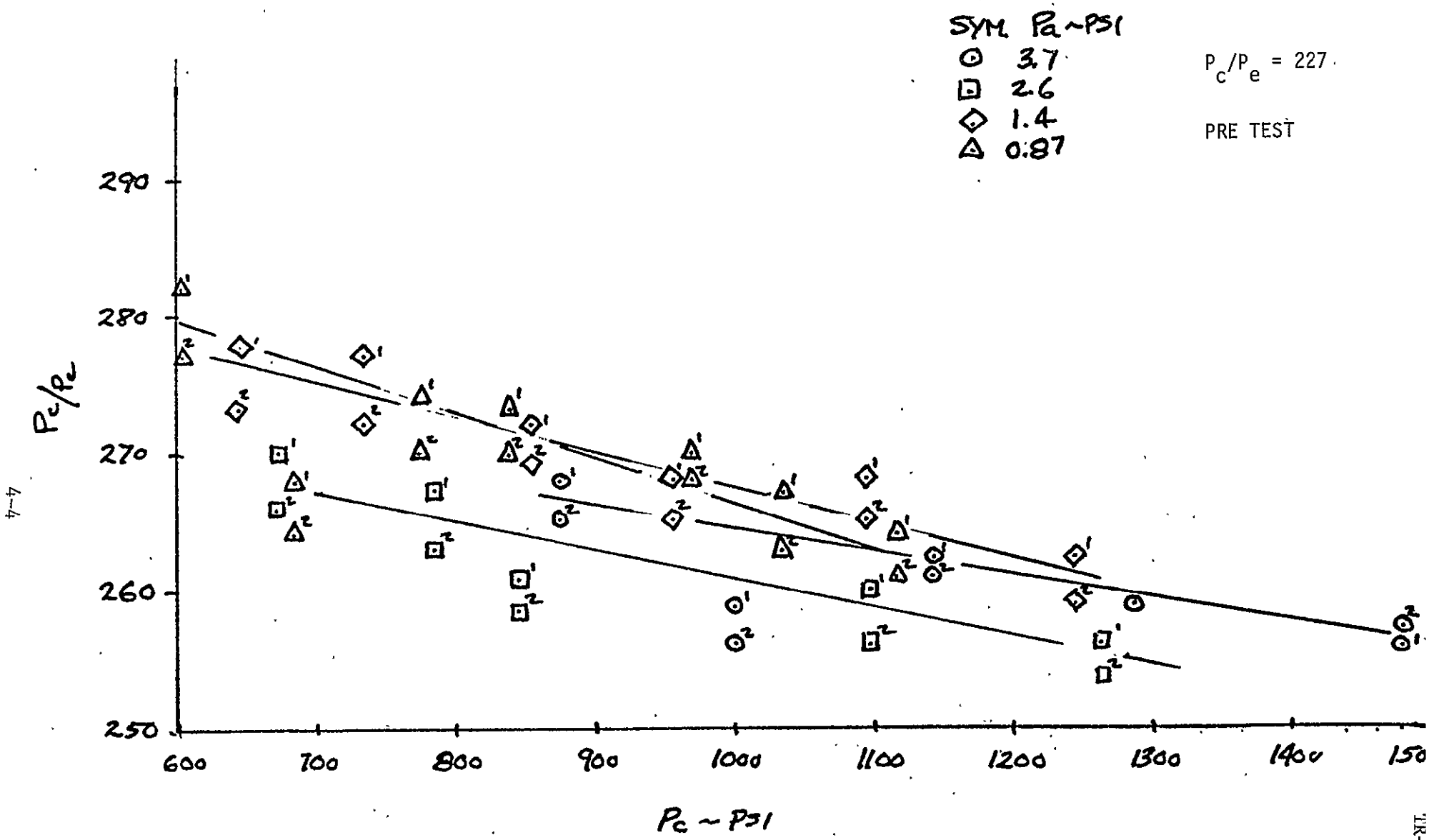
Figure 4-3. SSME NOZZLE CHAMBER TO EXIT PRESSURE RATIO — IA138
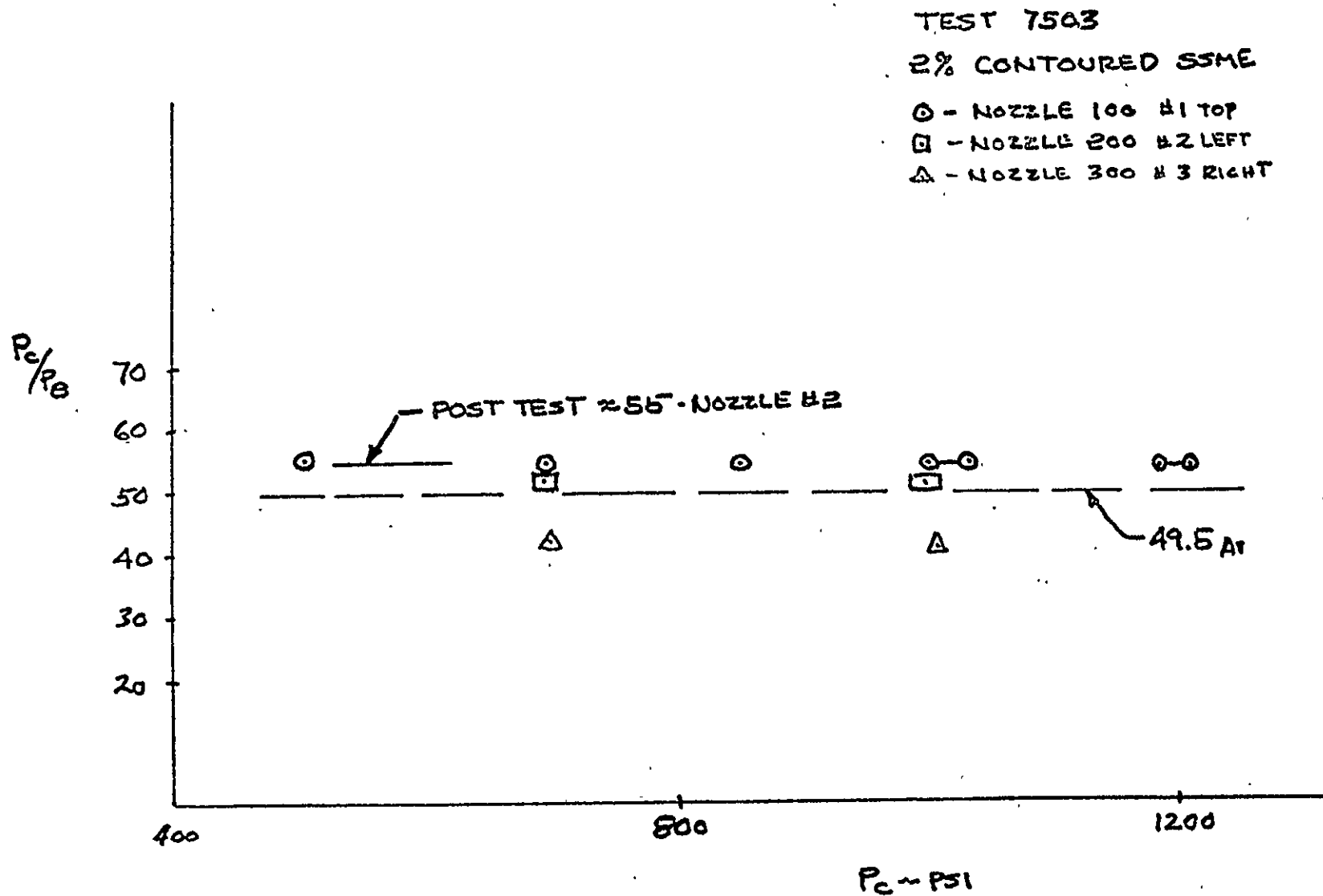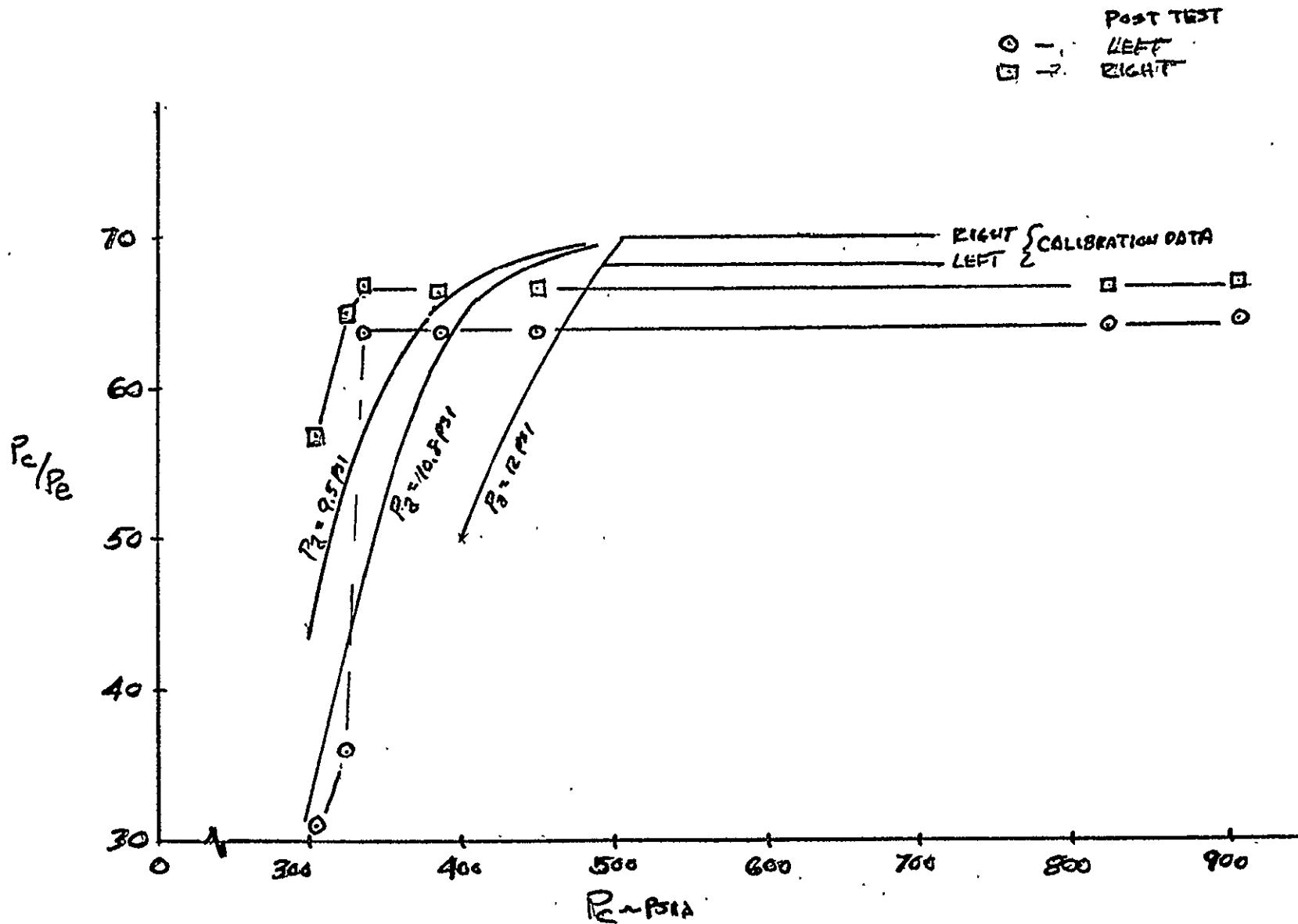
SYM. Pa~PSI
⊙ 3.76
⊡ 2.58
◈ 11.40
△ 0.87

90

80

P_a/P_e ~

70

60

⊥ PRE TEST

50
200   300   400   500   600   700   800   900

Pc ~ PSI
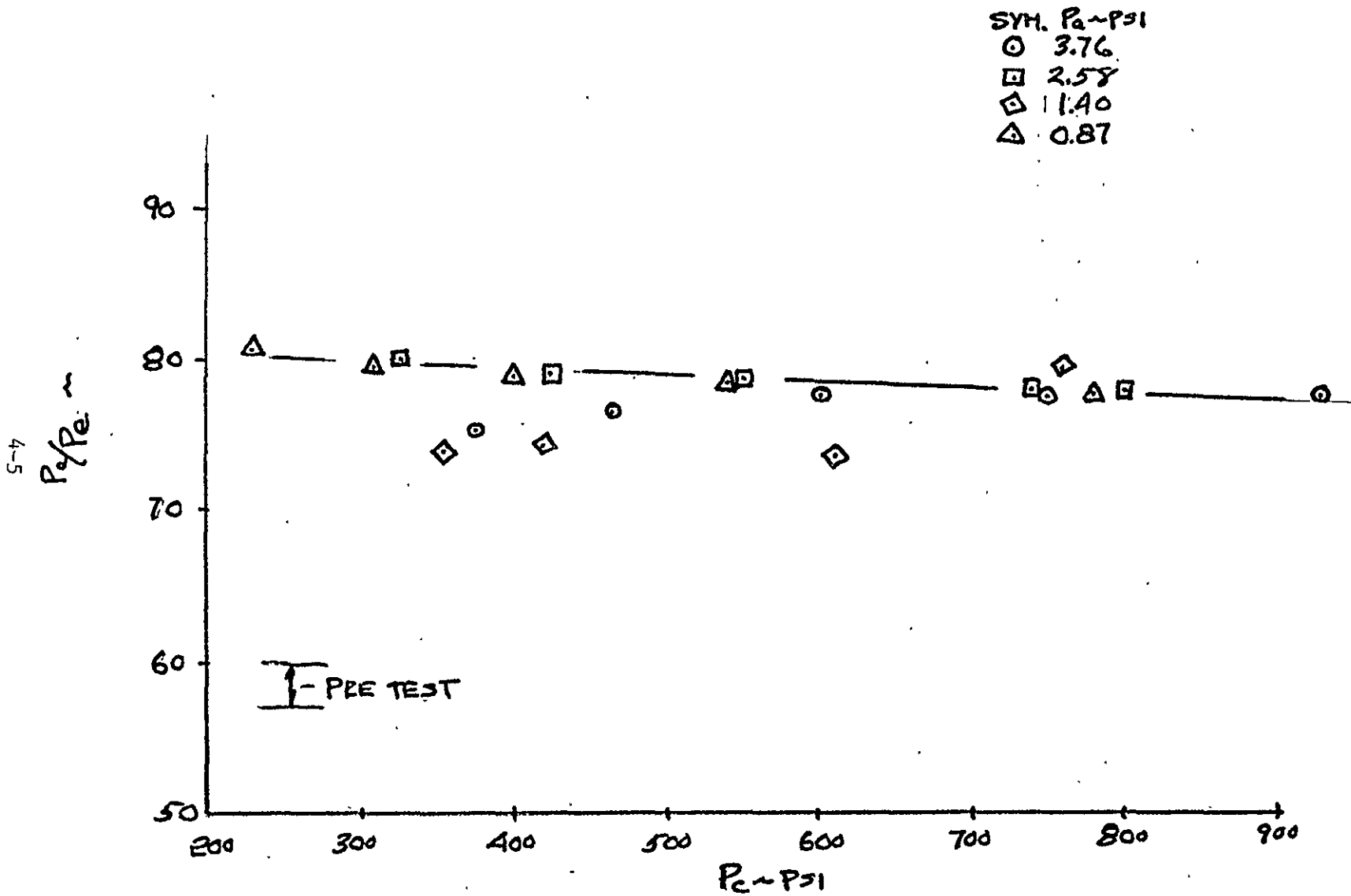
Figure 4-4.   SRB NOZZLE CHAMBER TO EXIT PRESSURE RATIO — IA138

TR-1964

Section V

PLUME SIMULATION

The Space Shuttle plumes were simulated using cold air flowing through model nozzles. The model plume characteristics required to develop base and forebody pressure environments were determined using an iteration procedure requiring the development of "PROTOTYPE POSSIBILITY CURVES". Prototype possibility curves are curves of base pressure or base pressure coefficient versus prototype plume characteristics. An example prototype possibility curve is shown in Figure 5-1. The curve is called possibility curve since it is developed for a range of possible prototype base pressure environments. These curves were developed prior to the wind tunnel test for both the SSME and SRB prototype nozzles. The SSME possibility curves were developed using possible orbiter base pressure coefficients and the SRB possibility curves were developed using SRB possible base pressure environments. During the power level portion of the test, model base pressure data are plotted on the prototype possibility curves as shown in Figure 5-1. The model power level is determined where the model pressure curve crosses the prototype pressure curve. An iteration procedure is used when there are two variables involved that influence the base pressure, i.e. SSME power level and SRB power level. The possibility curves and the model pressure data used to determine the nominal power levels at each Mach number are presented in the Appendix of references 1 and 2.

The form of the plume simulation equation used during the IA119 and IA138 test program was the following (reference 6)

$$\delta_j \gamma_j^N \Big|_{\text{PROT.}} = \delta_j \gamma_j^N \Big|_{\text{MODEL}}$$

where N is a function of Mach number. A plot of N versus Mach number is shown in Figure 5-2 and was obtained from reference 7. This curve was developed by correlating the base pressure in the near field and the far field developed from cold gas air and CF_4 plumes. The plume induced near field and far field areas considered are shown in Figure 5-3. The model configurations used were single body single nozzle, single body triple nozzle and triple body configurations. The triple body configuration was similar to the ET-SRB space shuttle

configuration. The band on the curve represents the range of N for the various
models used in the plume technology test (i.e., single body, triple body, etc.).
The criteria used for correlation of the plume technology data was that the
same base pressure occur for a five percent or less change in similarity
parameter. The band represents the total spread of N for the various model and
nozzle configurations considered in the plume technology program.

Recent analysis (Reference 8) has identified a new similarity parameter
that has the functional form

$$\frac{M_i \delta_i}{f(M_{EX}) \, g(\gamma_j)}$$

where f, g appear to depend weakly upon M_∞ and configuration.
The functions f and g have been defined for several model configurations and
Mach numbers. The form of the various base pressure correlation parameters is
presented in Table 5-1. These new similarity parameters, namely

$$\frac{M_i \delta_i}{M_E^{(.25)} \gamma_j}, \quad \frac{M_i \delta_i}{M_E^{(.25)} \gamma_j^{(.5)}}, \quad \text{and} \quad \frac{M_i \delta_i}{\gamma_j}$$ have been tabulated on the data pages

for the IA138 test results along with the value of $\delta_j \gamma_j^N$ (see Section VII).

$M_\infty \longrightarrow$

P_B

P_E

M_E

P_c

POSSIBILITY CURVE P_c = CONSTANT

TEST RESULTS P_c VARIED

P_B/P_∞

P_{c_2} MATCH POINT

P_{c_1}

SIMILARITY PARAMETER
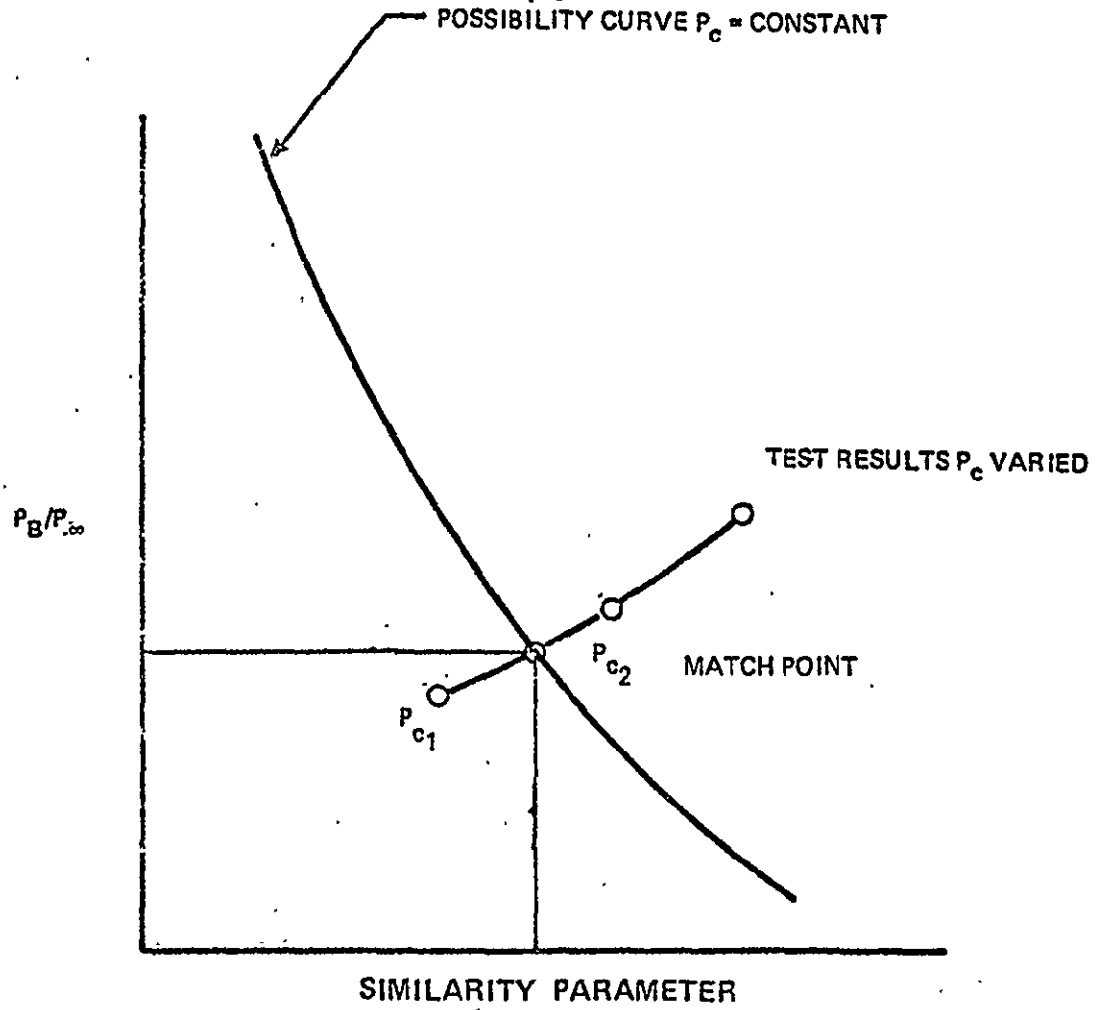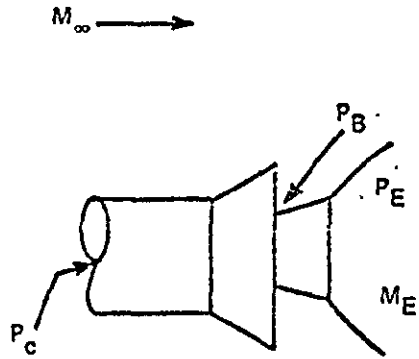
Figure 5-1.   PROTOTYPE POSSIBILITY CURVE

$$\delta_{j_B} \gamma_j^N$$
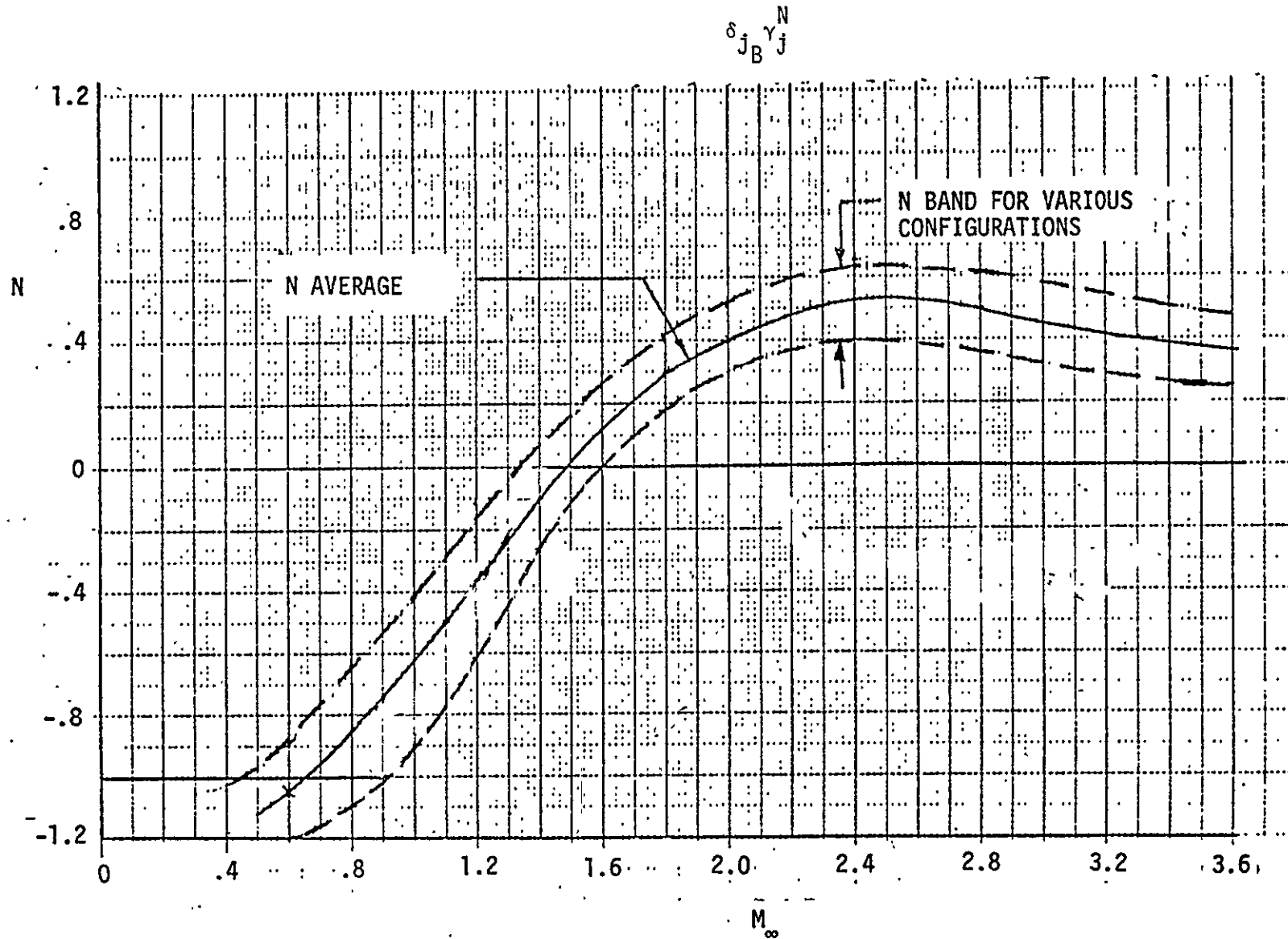
Figure 5-2. SIMILARITY PARAMETER EXPONENT
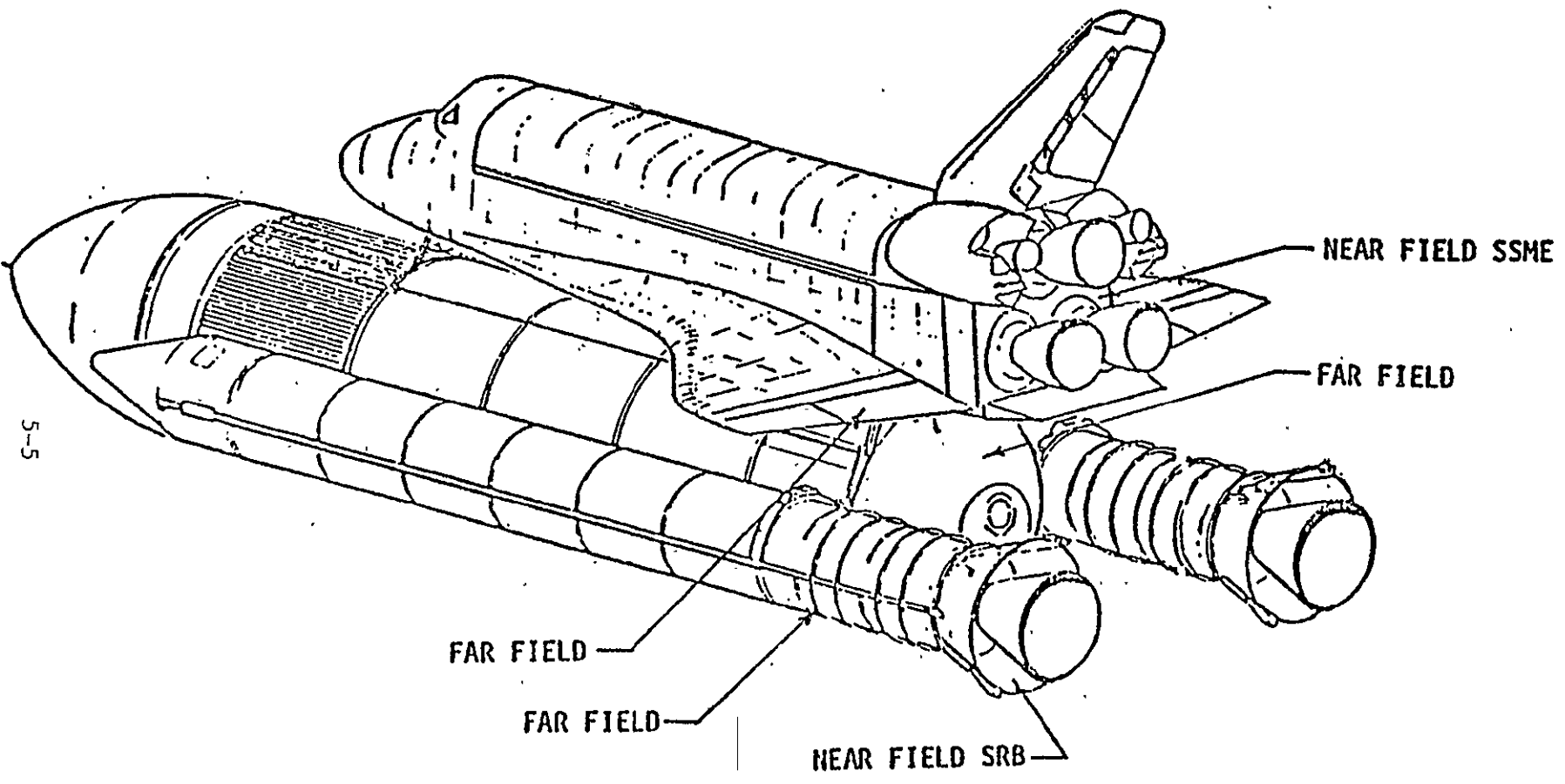
Figure 5-3. PLUME FLOW FIELD AREAS

NEAR FIELD SSME

FAR FIELD

FAR FIELD

FAR FIELD

NEAR FIELD SRB

Table 5-1
CORRELATION PARAMETERS

M_∞	CONFIGURATION		
	SINGLE BODY SINGLE NOZZLE	SINGLE BODY TRIPLE NOZZLE	TRIPLE BODY
0.9	$\dfrac{M_j \delta_j}{M_{EX}^{0.25} \gamma_j}$	$\dfrac{M_j \delta_j}{M_{EX}^{0.25} \gamma_j}$	$\dfrac{M_j \delta_j}{M_{EX}^{0.25} \gamma_j}$
1.2	$\dfrac{M_j \delta_j}{M_{EX}^{0.25} \gamma_j^{0.5}}$	$\dfrac{M_j \delta_j}{M_{EX}^{0.25} \gamma_j}$	$\dfrac{M_j \delta_j}{M_{EX}^{0.25} \gamma_j}$
1.46	$\dfrac{M_j \delta_j}{M_{EX}^{0.25} \gamma_j^{0.5}}$	$\dfrac{M_j \delta_j}{M_{EX}^{0.25} \gamma_j}$	
3.48	$\dfrac{M_j \delta_j}{\gamma_j}$	$\dfrac{M_j \delta_j}{\gamma_j}$	

Section VI

DATA ANALYSIS

Five computer codes were used to analyze the test data. These programs
are: 1. SORT program, 2. Power Delta program, 3. Sigma V Punch, 4. Wind
Tunnel Pressure Data Analysis and 5. Plume Integration. A brief discussion
of each of these programs is presented below.

SORT PROGRAM

The SORT Program was used to sort the run and sequence data sets into
basic groups of four. The four run groups consist of $+\beta$ power-on, $+\beta$ power-off,
$-\beta$ power-on and $-\beta$ power-off. The four run data sets were arranged in angle
of attack sets of -8, -4, 0, 4. Flags were set to note α, β, Mach, gimbal
and configuration incompatibility of the four run sets.

The following tolerances were put on the data sets to check compatibility.

VARIABLE	TOLERANCE
MACH	.03
α	.25
β	.25
β	Sign
Gimbal	$\neq 0$
CONFIGURATION NO. DO NOT AGREE	
RUN NUMBER/SEQUENCE OUT OF PLACE	
δ_{INB}	$\pm .25$
δ_{OUT}	$\pm .25$

The SORT program proved very useful in identifying errors in the post test
run schedule and differences between the power-on and power-off model
attitude.

POWER DELTA PROGRAM

The Power Delta program was used to evaluate the change in the pressure data due to power. The program lists all data from the power on run and all data from the power off run and then subtracts the two data sets and lists the power delta's. This allows a rapid survey of the power delta's·for abnormal numbers and a reference to the power on run and power off run to determine the error source.

SIGMA V PUNCH

The Sigma V Punch program was used in conjunction with the Power Delta program to sort the forebody power delta data into various elements and components and punch cards of the power delta in a format compatible with the "Wind Tunnel Pressure Data Analysis Program - WTPDA". WTPDA is an interactive graphic pressure data integration computer program which operates on the Sigma V Graphics System.

WIND TUNNEL PRESSURE DATA ANALYSIS (WTPDA)

WTPDA is an interactive computer graphics program which allows an engineer to·apply his judgement to the smoothing of wind tunnel pressure data in a real time environment. The purpose of the program is to produce airloads which are compatible with vehicle stability data and which reflect engineering judgement. WTPDA employs interactive computer techniques so that an engineer can develop balanced airloads in a timely manner.

WTPDA can integrate pressure data on wings, vertical stabilizers, fins, cylinders, and arbitrary cross-section fuselages. Although WTPDA was developed specifically to handle the Space Shuttle launch vehicle, it is capable of handling almost any arbitrary cross-section body.

The WTPDA·program was used to plot and smooth the power delta CP's on the forebody. Only limited integration of pressures were performed to check the main pressure integration computer program which is discussed below.

PLUME INDUCED PRESSURE INTEGRATION

The Plume Integration computer program was the main tool used to analyze the IA119 and IA135 pressure data. This computer program was developed

specifically to analyze the IA119 pressure data and was used to integrate the pressure data to obtain base and forebody plume induced aerodynamic loads and moments. The computer program was developed to analyze four run sequences of positive and negative β sets. This operation is required since portions of the model have pressure data on only one side. Thus, to analyze the effects of sideslip required the evaluation of + and - β runs. Both power-on and power-off data sets are required since a portion of the plume induced data uses power on pressure coefficients while other portions require only the change in pressure coefficient due to power.

The analysis of the plume induced aerodynamic characteristics was performed using different pressure data over different portions of the vehicle. This type of analysis was required because of the unique configuration of the Space Shuttle and the model configurations used to obtain the forebody aerodynamic characteristics. The two types of pressure data used for analysis are: 1) The power on C_p's for nominal SSME and SRB model power settings; and 2) The power delta C_p's where $\Delta C_{p_{Power}} = C_{p_{Power\ on}} - C_{p_{Power\ off}}$.

The power on C_p's were used to evaluate the power-on base forces and moments. The power delta C_p's were used to evaluate the change-in forebody aerodynamic characteristics. The location on the Space Shuttle vehicle where the different types of pressure data were used is shown in Figure 6-1. The results of integration of the base pressure and the forebody power delta pressures have been listed in a special format which is discussed in Section VII.
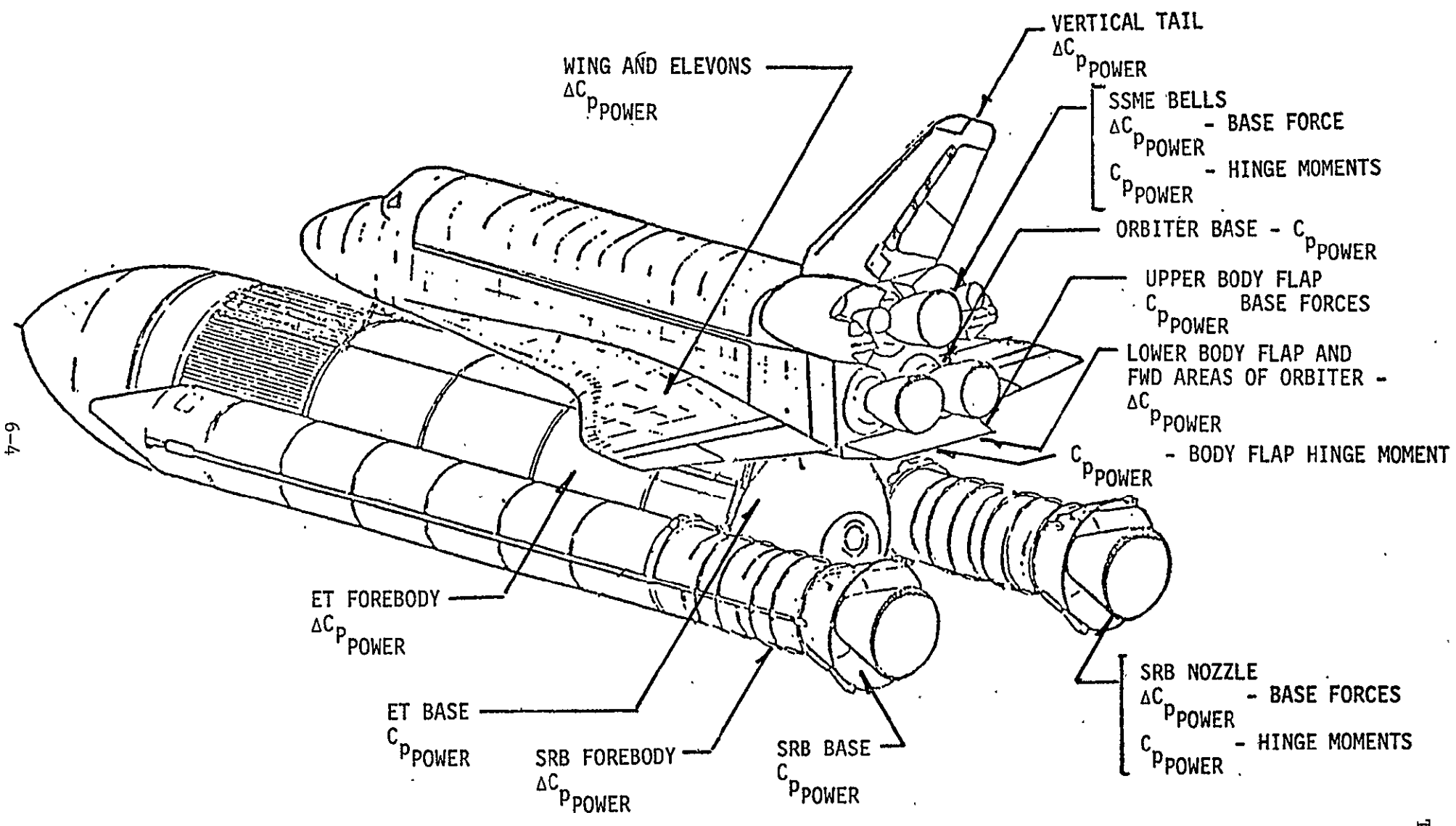
Figure 6-1. PLUME FLOW FIELD AREAS

VERTICAL TAIL $\Delta C_{p_{POWER}}$

SSME BELLS
$\Delta C_{p_{POWER}}$ - BASE FORCE
$C_{p_{POWER}}$ - HINGE MOMENTS

WING AND ELEVONS $\Delta C_{p_{POWER}}$

ORBITER BASE - $C_{p_{POWER}}$

UPPER BODY FLAP $C_{p_{POWER}}$ BASE FORCES

LOWER BODY FLAP AND FWD AREAS OF ORBITER - $\Delta C_{p_{POWER}}$

$C_{p_{POWER}}$ - BODY FLAP HINGE MOMENT

ET FOREBODY $\Delta C_{p_{POWER}}$

ET BASE $C_{p_{POWER}}$

SRB FOREBODY $\Delta C_{p_{POWER}}$

SRB BASE $C_{p_{POWER}}$

SRB NOZZLE
$\Delta C_{p_{POWER}}$ - BASE FORCES
$C_{p_{POWER}}$ - HINGE MOMENTS

TR-1964

Section VII

TEST RESULTS

The results of the integration of the base pressure and forebody power delta's are presented in table form in the Appendix of references 1 and 2. The output of the Plume Integration computer program contains all the results of the pressure integration including base coefficients, forces and moments and forebody coefficient data from pressure integration along with the gage data.

An example of the printout of a data set from test IA119 is presented below. The data are arranged in 9 sections. Section 1 presents the run numbers, Mach number, vehicle configuration, and attitude. Section 2 presents the nozzle gas dynamic properties. Section 3 presents the nozzle gas dynamic similarity parameter. Section 4 presents the results of the pressure integration over the base elements and components. Section 5 presents the average base pressure coefficient for each element. Section 6 presents the nozzle average base pressure coefficients. Section 7 presents the nozzle hinge moment data. Section 8 presents the forebody data from the gages. Section 9 presents the forebody data from pressure integration.

IA119 TEST DATA FORMAT

Printouts of each run sequence set is presented in the Appendix of reference 1. The data sets are grouped for a constant Mach number. The first data set within a Mach group is the power-off runs. The second group contains the variable power runs. The third group are the various elevon deflections. The fourth group contains the various gimbal angle runs and the fifth group is a 90° roll run sets.

An example of the printout of a data set from test IA138 is presented below. The data are arranged in 9 sections. Section 1 presents the run numbers, Mach number, vehicle configuration and attitude. Section 2 presents the nozzle gas dynamic properties. Section 3 presents the plume gas dynamic similarity parameters. Section 4 presents the values of parameters used to determine the similarity parameters. Section 5 presents the results of the pressure integration over the base of the elements and components. Section 6 presents the average base pressure coefficient for each element. Section 7 presents the nozzle average base pressure coefficients. Section 8 presents the forebody data from the gages. Section 9 presents the forebody data from pressure integration.

IA138 TEST DATA FORMAT

Printouts of each run sequence set is presented in the appendix of reference 2. The data sets are grouped for a constant Mach number. The first data set within a Mach group is the power-off runs. The second group contains the variable power runs and the third group contains the various elevon deflections.

The base and forebody plume induced data tabulated on the printout sheets were analyzed and developed into math models. The math model is a description of the nominal aerodynamic data and a tolerance model. The math model of the base plume induced aerodynamic characteristics is presented in Section VIII. The math model of the forebody plume induced aerodynamic characteristics is presented in Section IX.

Section VIII

BASE MATH MODEL

A math model of the base plume induced aerodynamic characteristics was developed which can be used in conjunction with the forebody aerodynamic characteristics to evaluate the aerodynamic characteristics of the total space shuttle launch vehicle and each element. Three types of base aerodynamic characteristics were developed. These include 1. SSLV and element base aerodynamic coefficients for Mach numbers from 0.6 to 2.5, 2. SSLV base forces and moments versus altitude up to 160,000 ft. and 3. SSLV and element base coefficient tolerances for Mach numbers from 0.6 to 2.5. The math model consists of a description of the base aerodynamic coefficients at a given Mach number and elevon deflection for various α, β values. Gradients are provided giving the change in the aerodynamic characteristics with the two primary variables that influence the base flow (inboard elevon deflection and SSME power level).

The base aerodynamic math model is limited to the base axial force, normal force and pitching moment. Lateral-directional forces and moments exist on some base components, but no consistent trend could be identified and thus they are included in the base tolerance model. Base coefficients and tolerances for each element are provided for Mach numbers from 0.6 to 2.5. The base aerodynamic coefficient math model is described by the following equation,

$$C_{x_i} = [C_{x_i}]_{\alpha,\beta} + [\partial C_{x_i}/\partial \delta_{EI}] \times \Delta \delta_{EI} + [\partial C_{x_i}/\partial \% \text{ SSME POWER}] \times (\Delta \% \text{ SSME POWER})$$

where $[C_{x_i}]_{\alpha,\beta}$ is a 4x7 matrix for $\alpha = +4,0,-4,-8$
$\beta = -6,-4,-2,0,2,4,6$

elevon deflection corresponds to close schedule 6

i = SSLV, ORBITER, ET, LEFT SRB, RIGHT SRB

$\partial C_{x_i}/\partial \delta_{EI}$ Gradient for inboard elevon deflection - function of Mach number only

i = SSLV, ORBITER, ET

8-1

$\partial C_{x_i}/\partial$SSME POWER
  Gradient for percent change in SSME power level - function of Mach number only

  i = SSLV,ORBITER

$\Delta\delta_{EI}$ - Change in inboard elevon deflection from math model value to inboard elevon deflection of interest.

Δ%SSME POWER LEVEL - Change in percent SSME power level from math model value to SSME power level of interest

Typical values of the coefficient $[C_{x_i}]_{\alpha,\beta}$ are presented in Tables 8-1, 8-2, and 8-3 for each element and the total SSLV vehicle. Typical values of the coefficient gradients are presented in Table 8-4.

Base forces and moments have been determined versus altitude using the base coefficient math model. The base force math model is for the total vehicle and uses the following model,

$$\left.\begin{matrix}F\\M\end{matrix}\right|_{ALT} = \left.\begin{matrix}F\\M\end{matrix}\right|_{\alpha=0} + \left[\frac{\partial F}{\partial \alpha}\right] \times \alpha + \left[\frac{\partial F_X}{\partial \delta_{EI}}\right]\Delta\delta_{EI} + \frac{\partial F}{\partial\%\,SSME\,POWER} \times (\Delta\%\,SSME\,POWER)$$

where:

$\left.\begin{matrix}F\\M\end{matrix}\right|_{\alpha=0}$
  SSLV base force or moment - function of altitude only

$[\partial F/\partial\alpha]$ Gradient for angle of attack - function of only altitude

$[\partial F/\partial\delta_{EI}]$ Gradient for inboard elevon deflection - function of altitude only

$[\partial F/\partial\%SSME\,POWER]$ Gradient for percent change in SSME power level

α angle of attack

$\Delta\delta_{EI}$ Change in inboard elevon deflection from math model value to inboard elevon deflection of interest

Δ%SSME POWER level   Change in percent SSME power level from math
model value to SSME power level of interest.

Typical values of the base axial force, normal force and pitching moment are
presented in Tables 8-5, 8-6, and 8-7. Typical values of the base force partials
are presented in Table 8-8.

BASE COEFFICIENT TOLERANCES

Examples of the base coefficient tolerances are presented in Tables 8-9 and
8-10. The coefficient tolerances cover all attitudes and configurations from
the base coefficients presented in the math model to flight data and are to a
+3σ level. The moment tolerances are considered to be only due to force
tolerances. The moment tolerance due to the aerodynamic center location
uncertainty being a smaller order of magnitude. Examples of the base moment
coefficient increment equations are presented in Table 8-10.

The base tolerances include contributions due to 1. test instrumentation
uncertainty, 2. simulation parameter uncertainty, 3. Reynolds number
characteristics, 4. Model-tunnel testing uncertainties, 5. Pressure integra-
tion uncertainties and 6. Math model uncertainties. Each tolerance contribu-
tion is assumed independent and therefore the contributions are combined using
the RSS technique. The tolerances thus cover the uncertainty from the math model
to flight data and are to a +3σ level with a Gaussian distribution.

The model instrumentation contribution included the accuracy of the
Scanivalve^R calculations. The general accuracy is estimated to be $C_p = \pm.013$
for values of C_p in the range of ±.5. The general uncertainty of the
measured pressure coefficients was assumed to be 3%.

The simulation parameter uncertainty was assumed to be due to an uncer-
tainty in the exponent. The estimated uncertainty in the exponent is shown
in Figure 5-2. The exponent uncertainty was converted to an error in simulation
that generally represented a 10 percent uncertainty in base force coefficients.
The Reynolds number-scale uncertainty was obtained using past flight test to
wind-tunnel test results. This factor is a judgement factor and includes the
differences between the Saturn V and Titan 3C flight and wind tunnel data,

reduced to account for the plume technology program learning curve. This factor also includes a hot flow simulation uncertainty factor. The Reynolds number-scale uncertainty was generally 10% of the nominal base coefficient.

Model configuration uncertainties includes the effect of the support stings that will influence the flow field at angles of sideslip along with uncertainties due to other model configuration inaccuracies that potentially influence the local flow fields. Uncertainties due to model configuration similitude were approximately 7% of the nominal force coefficients.

Integration uncertainties included the potential error involved in the integration technique and represent approximately 3 percent of the nominal force coefficients.

The math model uncertainty included the errors of independent variables in the math model of the base forces and moments. Independent variables not included in the math model of the base forces and moments include nozzle gimbal angle and outboard elevon position.

The technique that was used to develop the SSLV base tolerances was to correlate the SRB and ET base tolerances and RSS those to the orbiter base coefficient tolerance. This procedure was used for the base axial force and normal force coefficients. The SSLV base side force coefficient was obtained by using the RSS technique for each element.

· The forebody plume induced aerodynamic characteristics were developed in conjunction with the base plume induced aerodynamic characteristics to allow a complete description of the plume induced characteristics of the Space Shuttle Launch Vehicle. The forebody plume induced aerodynamic characteristics are presented in Section IX.

Table 8-1.

BASE AXIAL FORCE COEFFICIENT

$M_\infty = 1.55$ $\delta_{e_{IO}} = 10/-2$

% SSME POWER = 109%

ELEMENT		α	β −6	−4	−2	0	2	4	6
CA-10L	1.55	−6.	.0685	.0663	.0642	.0625	.0642	.0663	.0685
CA-10L	1.55	−4.	.0646	.0632	.0616	.0605	.0616	.0632	.0646
CA-10L	1.55	−2.	.0629	.0616	.0601	.0591	.0601	.0616	.0629
CA-10L	1.55	0.	.0614	.0602	.0588	.0579	.0568	.0602	.0614
CA-10L	1.55	2.	.0595	.0583	.0571	.0561	.0571	.0583	.0595
CA-10L	1.55	4.	.0575	.0563	.0553	.0543	.0553	.0563	.0575
CA-10L	1.55	6.	.0557	.0546	.0534	.0525	.0534	.0546	.0557
CA-ORB	1.55	−6.	.0191	.0194	.0198	.0202	.0198	.0194	.0191
CA-ORB	1.55	−4.	.0194	.0197	.0200	.0204	.0200	.0197	.0194
CA-ORB	1.55	−2.	.0195	.0197	.0198	.0200	.0198	.0197	.0195
CA-ORB	1.55	0.	.0196	.0196	.0196	.0196	.0196	.0196	.0196
CA-ORB	1.55	2.	.0194	.0193	.0192	.0191	.0192	.0193	.0194
CA-ORB	1.55	4.	.0191	.0189	.0187	.0185	.0187	.0189	.0191
CA-ORB	1.55	6.	.0189	.0186	.0182	.0179	.0182	.0186	.0189
CA-ET	1.55	−6.	.0386	.0368	.0349	.0331	.0349	.0368	.0386
CA-ET	1.55	−4.	.0365	.0346	.0326	.0307	.0326	.0346	.0365
CA-ET	1.55	−2.	.0363	.0342	.0321	.0301	.0321	.0342	.0363
CA-ET	1.55	0.	.0361	.0340	.0318	.0297	.0318	.0340	.0361
CA-ET	1.55	2.	.0357	.0336	.0315	.0294	.0315	.0336	.0357
CA-ET	1.55	4.	.0351	.0331	.0312	.0292	.0312	.0331	.0351
CA-ET	1.55	6.	.0346	.0327	.0309	.0290	.0309	.0327	.0346
CA-R	1.55	−6.	.0078	.0067	.0056	.0046	.0039	.0034	.0030
CA-R	1.55	−4.	.0072	.0064	.0055	.0047	.0035	.0025	.0015
CA-R	1.55	−2.	.0064	.0058	.0051	.0045	.0031	.0019	.0007
CA-R	1.55	0.	.0057	.0052	.0047	.0043	.0027	.0014	.0000
CA-R	1.55	2.	.0050	.0046	.0042	.0038	.0022	.0008	−.0006
CA-R	1.55	4.	.0044	.0040	.0037	.0033	.0017	.0003	−.0011
CA-R	1.55	6.	.0038	.0035	.0031	.0028	.0012	−.0002	−.0016
CA-L	1.55	−6.	.0030	.0034	.0039	.0046	.0056	.0067	.0078
CA-L	1.55	−4.	.0015	.0025	.0035	.0047	.0055	.0064	.0072
CA-L	1.55	−2.	.0007	.0019	.0031	.0045	.0051	.0058	.0064
CA-L	1.55	0.	.0000	.0014	.0027	.0043	.0047	.0052	.0057
CA-L	1.55	2.	−.0006	.0008	.0022	.0038	.0042	.0046	.0050
CA-L	1.55	4.	−.0011	.0003	.0017	.0033	.0037	.0040	.0044
CA-L	1.55	6.	−.0016	−.0002	.0012	.0028	.0031	.0035	.0038

Table 8-2.

M$_\infty$ = 1.55 $\delta_{e_{IO}}$ = 10/-2

BASE NORMAL FORCE COEFFICIENT

% SSME POWER = 109%

ELEMENT	α	β -6	-4	-2	0	2	4	6
CN-IOL	1.55	-6.	.0135	.0135	.0135	.0135	.0135	.0135	.0135
CN-IOL	1.55	-4.	.0139	.0138	.0138	.0136	.0138	.0138	.0139
CN-IOL	1.55	-2.	.0141	.0138	.0138	.0136	.0136	.0138	.0141
CN-IOL	1.55	0.	.0141	.0139	.0135	.0133	.0135	.0139	.0141
CN-IOL	1.55	2.	.0140	.0138	.0137	.0135	.0137	.0138	.0140
CN-IOL	1.55	4.	.0138	.0138	.0138	.0138	.0138	.0138	.0138
CN-IOL	1.55	6.	.0137	.0138	.0139	.0140	.0139	.0138	.0137
CN-ORB	1.55	-6.	.0131	.0132	.0132	.0133	.0132	.0132	.0131
CN-ORB	1.55	-4.	.0138	.0137	.0136	.0134	.0136	.0137	.0138
CN-ORB	1.55	-2.	.0141	.0138	.0136	.0134	.0136	.0138	.0141
CN-ORB	1.55	0.	.0143	.0140	.0136	.0133	.0136	.0140	.0143
CN-ORB	1.55	2.	.0140	.0137	.0135	.0133	.0135	.0137	.0140
CN-ORB	1.55	4.	.0137	.0135	.0134	.0132	.0134	.0135	.0137
CN-ORB	1.55	6.	.0134	.0133	.0132	.0132	.0132	.0133	.0134
CN-ET	1.55	-6.	.0000	.0000	.0000	.0000	.0000	.0000	.0000
CN-ET	1.55	-4.	.0000	.0000	.0000	.0000	.0000	.0000	.0000
CN-ET	1.55	-2.	.0000	.0000	.0000	.0000	.0000	.0000	.0000
CN-ET	1.55	0.	.0000	.0000	.0000	.0000	.0000	.0000	.0000
CN-ET	1.55	2.	.0000	.0000	.0000	.0000	.0000	.0000	.0000
CN-ET	1.55	4.	.0000	.0000	.0000	.0000	.0000	.0000	.0000
CN-ET	1.55	6.	.0000	.0000	.0000	.0000	.0000	.0000	.0000
CN-R	1.55	-6.	.0001	.0001	.0001	.0001	.0002	.0002	.0003
CN-R	1.55	-4.	.0001	.0001	.0001	.0001	.0001	.0000	-.0000
CN-R	1.55	-2.	-.0000	.0000	.0000	.0001	.0000	-.0000	-.0000
CN-R	1.55	0.	-.0002	-.0001	-.0001	-.0000	.0000	-.0000	-.0000
CN-R	1.55	2.	.0001	.0001	.0001	.0001	.0001	-.0000	-.0001
CN-R	1.55	4.	.0003	.0003	.0003	.0003	.0001	-.0000	-.0002
CN-R	1.55	6.	.0006	.0005	.0005	.0004	.0002	-.0000	-.0003
CN-L	1.55	-6.	.0003	.0002	.0002	.0001	.0001	.0001	.0001
CN-L	1.55	-4.	-.0000	.0000	.0001	.0001	.0001	.0001	.0001
CN-L	1.55	-2.	-.0000	-.0000	.0000	.0001	.0000	.0000	-.0000
CN-L	1.55	0.	-.0000	-.0000	.0000	-.0000	-.0001	-.0001	-.0002
CN-L	1.55	2.	-.0001	-.0000	.0001	.0001	.0001	.0001	.0001
CN-L	1.55	4.	-.0002	-.0000	.0001	.0003	.0003	.0003	.0003
CN-L	1.55	6.	-.0003	-.0000	.0002	.0004	.0005	.0005	.0006

Table 8-3. $M_\infty = 1.55$ $\delta_{e_{IO}} = 10/-2$

BASE PITCHING MOMENT COEFFICIENT   % SSME POWER = 109%

ELEMENT	α	β -6	-4	-2	0	2	4	6
CM-IOL	1.55	-6.	-.0063	-.0063	-.0063	-.0062	-.0063	-.0063	-.0063
CM-IOL	1.55	-4.	-.0067	-.0065	-.0064	-.0062	-.0064	-.0065	-.0067
CM-IOL	1.55	-2.	-.0067	-.0065	-.0064	-.0062	-.0064	-.0065	-.0067
CM-IOL	1.55	0.	-.0064	-.0063	-.0061	-.0060	-.0061	-.0063	-.0064
CM-IOL	1.55	2.	-.0065	-.0065	-.0064	-.0063	-.0064	-.0065	-.0065
CM-IOL	1.55	4.	-.0065	-.0066	-.0067	-.0068	-.0067	-.0066	-.0065
CM-IOL	1.55	6.	-.0065	-.0068	-.0070	-.0071	-.0070	-.0068	-.0065
CM-ORB	1.55	-6.	-.0058	-.0059	-.0059	-.0060	-.0059	-.0059	-.0058
CM-ORB	1.55	-4.	-.0063	-.0062	-.0061	-.0060	-.0061	-.0062	-.0063
CM-ORB	1.55	-2.	-.0065	-.0063	-.0062	-.0060	-.0062	-.0063	-.0065
CM-ORB	1.55	0.	-.0066	-.0064	-.0062	-.0060	-.0062	-.0064	-.0066
CM-ORB	1.55	2.	-.0064	-.0063	-.0062	-.0061	-.0062	-.0063	-.0064
CM-ORB	1.55	4.	-.0062	-.0062	-.0062	-.0062	-.0062	-.0062	-.0062
CM-ORB	1.55	6.	-.0060	-.0061	-.0062	-.0063	-.0062	-.0061	-.0060
CM-ET	1.55	-6.	.0000	.0000	.0000	.0000	.0000	.0000	.0000
CM-ET	1.55	-4.	.0000	.0000	.0000	.0000	.0000	.0000	.0000
CM-ET	1.55	-2.	.0000	.0000	.0000	.0000	.0000	.0000	.0000
CM-ET	1.55	0.	.0000	.0000	.0000	.0000	.0000	.0000	.0000
CM-ET	1.55	2.	.0000	.0000	.0000	.0000	.0000	.0000	.0000
CM-ET	1.55	4.	.0000	.0000	.0000	.0000	.0000	.0000	.0000
CM-ET	1.55	6.	.0000	.0000	.0000	.0000	.0000	.0000	.0000
CM-R	1.55	-6.	-.0002	-.0002	-.0002	-.0001	-.0002	-.0002	-.0003
CM-R	1.55	-4.	-.0003	-.0002	-.0002	-.0001	-.0001	-.0001	-.0001
CM-R	1.55	-2.	-.0001	-.0001	-.0001	-.0001	-.0001	-.0001	-.0001
CM-R	1.55	0.	.0002	.0001	.0001	.0000	-.0000	-.0000	.0000
CM-R	1.55	2.	-.0002	-.0002	-.0001	-.0001	-.0001	.0000	.0001
CM-R	1.55	4.	-.0005	-.0004	-.0004	-.0003	-.0001	.0000	.0002
CM-R	1.55	6.	-.0008	-.0007	-.0006	-.0004	-.0002	.0000	.0003
CM-L	1.55	-6.	-.0003	-.0002	-.0002	-.0001	-.0002	-.0002	-.0002
CM-L	1.55	-4.	-.0001	-.0001	-.0001	-.0001	-.0002	-.0002	-.0003
CM-L	1.55	-2.	-.0001	-.0001	-.0001	-.0001	-.0001	-.0001	-.0001
CM-L	1.55	0.	.0000	-.0000	-.0000	.0000	.0001	.0001	.0002
CM-L	1.55	2.	.0001	.0000	-.0001	-.0001	-.0001	-.0002	-.0002
CM-L	1.55	4.	.0002	.0000	-.0001	-.0003	-.0004	-.0004	-.0005
CM-L	1.55	6.	.0003	.0000	-.0002	-.0004	-.0006	-.0007	-.0008

Table 8-4

BASE COEFFICIENT PARTIALS

	MACH	$\partial C_{x_i}/\partial\delta_{EI}$			$[\partial C_{x_i}/\partial\% \text{ SSME POWER}] \times 10$	
		SSLV	ORBITER	ET	SSLV	ORBITER
CA	600	.0025	-.0003	.0028	.0007	.0007
CA	1050	.0040	.0002	.0038	.0010	.0010
CA	1100	.0018	.0003	.0015	.0008	.0008
CA	1250	.0000	.0001	-.0001	.0010	.0010
CA	1400	.0000	.0000	.0000	-.0006	-.0006
CN	600	.0000	.0000	.0000	.0002	.0002
CN	1050	.0001	.0001	.0000	.0005	.0005
CN	1100	.0001	.0001	.0000	.0004	.0004
CN	1250	.0001	.0001	.0000	.0004	.0004
CN	1400	.0001	.0001	.0000	-.0003	-.0003
CM	600	.0000	.0000	.0000	-.0001	-.0001
CM	1050	-.0001	-.0001	.0000	-.0002	-.0002
CM	1100	-.0001	-.0001	.0000	-.0002	-.0002
CM	1250	-.0001	-.0001	.0000	-.0002	-.0002
CM	1400	-.0001	-.0001	.0000	.0001	.0001

Table 8-5

BASE AXIAL FORCE (LBS)

ALTITUDE (ft)	TOTAL	NOMINAL % SSME POWER LEVEL	ALTITUDE (ft)	TOTAL	NOMINAL % SSME POWER LEVEL
0	0	109	52500	46240	109
4000	41295	109	55000	33015	
6000	112146	109	57500	27690	
8000	148363	109	60000	19389	
10000	162595	107	62500	12579	
12000	178724	101	65000	7039	
14000	193983	95	67500	2504	
16000	209734	88.4	70000	-2022	
18000	226100		72500	-5026	
19000	240776		75000	-7416	
20000	257649		77500	-9434	
21000	309484		80000	-10837	
22000	341482		85000	-12161	
23000	354185		90000	-12341	
24000	357716		95000	-12191	
25000	338036		100000	-11700	
26000	294479		110000	-10812	
28000	256747	↓	120000	-9258	
30000	230650	88.4	130000	-7641	
34000	193188	93	140000	-7074	
38000	157365	105	145000	-6554	↓
42000	107143	109	160000	-6334	109
44000	91278.				
46000	78961				
48000	67757	↓			
50000	56630	109			

Table 8-6

BASE NORMAL FORCE (LBS)

ALTITUDE (ft)	TOTAL	NOMINAL % SSME POWER LEVEL	ALTITUDE (ft)	TOTAL	NOMINAL % SSME POWER LEVEL
0	0	109	47500	15315	109
5000	18500	109	50000	12685	
10000	24966	107	52500	10322	
12000	26867	101	55000	8303	
14000	28381	95	57500	6785	
16000	30163	88.4	60000	5476	
18000	32278		62500	4500	
19000	33678		65000	3900	
20000	36009		67500	2700	
21000	41054		70000	2090	
22000	48096		75000	1175	
23000	50853		80000	391	
24000	51688		85000	-193	
25000	50621		90000	-565	
26000	45343		95000	-791	
28000	40842		100000	-1023	
30000	39239	88.4	110000	-1221	
34000	35678	93	120000	-1380	
38000	28850	105	130000	-1384	
40000	25704	109	140000	-1451	
42500	21982	109	150000	-1500	
450000	18546	109	160000	-1400	109

Table 8-7

BASE PITCHING MOMENT (FT. LBS)

ALTITUDE (ft)	PITCHING MOMENT (ft-lbs)	NOMINAL % SSME POWER LEVEL	ALTITUDE (ft)	PITCHING MOMENT (ft-lbs)	NOMINAL % SSM POWER LEVEL
0	0	109	47500	-995473	109
5000	-1220000	109	50000	-828630	
10000	-1296826	107	52500	-684740	
12000	-1374159	101	55000	-563750	
14000	-1441528	95	57500	-462600	
16000	-1484908	88.4	60000	-385320	
18000	-1535100	↓	62500	-320000	
19000	-1589046		65000	-250000	
20000	-1701877		67500	-200000	
21000	-1937440		70000	-159200	
22000	-2206003		75000	-38110	
23000	-2218121		80000	-39080	
24000	-2187319		85000	-4825	
25000	-2101904		90000	14130	
26000	-1942585		95000	41395	
28000	-1785366	↓	100000	55800	
30000	-1713072	88.4	110000	72303	
34000	-1515453	93	120000	82300	
38000	-1202968	105	130000	84635	
40000	-1750000	109	140000	88920	
42500	-1458720	109	150000	95000	↓
45000	-1232990	109	160000	95000	109

Table 8-8

BASE AXIAL FORCE PARTIALS

ALTITUDE (ft)	$\partial AF/\partial \alpha$ (LB/DEG)	$\partial AF/\partial \delta_{EI}$ (LB/DEG)	$\partial AF/\partial \%$ SSME POWER (LB/%)
10000	-1331.0	2623.0	73.0
12000	-1361.0	2959.0	71.0
14000	-1536.0	3255.0	62.0
16000	-1823.0	3665.0	43.0
18000	-2454.0	5653.0	26.0
19000	-2667.0	6400.0	23.0
20000	-2716.0	7761.0	31.0
21000	-2021.0	8842.0	107.0
22000	-705.0	9138.0	138.0
23000	1040.0	9098.0	159.0
24000	2461.0	8533.0	167.0
25000	3148.0	6959.0	169.0
26000	2911.0	4350.0	167.0
28000	1627.0	1864.0	142.0
30000	514.0	171.0	158.0
34000	-583.0	87.0	96.0
38000	-1014.0	21.0	-112.0

Table 8-9

IA-119
BASE COEFFICIENT TOLERANCES

$\pm\Delta C_A$

MACH NO.	SSLV	ORB	ET	SRB(1)
.6	.0104	.0031	.0065	.0017
.8	.0107	.0031	.0072	.0015
.9	.0156	.0046	.0107	.0021
.95	.0359	.0088	.0270	.0039
1.05	.0239	.0080	.0161	.0032
1.10	.0169	.0057	.0115	.0022
1.15	.0133	.0046	.0091	.0017
1.25	.0086	.0033	.0060	.0010
1.40	.0062	.0024	.0045	.0006
1.55	.0069	.0032	.0050	.0006
1.80	.0082	.0054	.0050	.0006
2.20	.0078	.0050	.0044	.0008
2.50	.0070	.0040	.0040	.0009

$\pm\Delta C_N$ *

$*\Delta C_{N_O} = 0.6 \ \Delta C_{A_O}$

	SSLV	ORB	ET	SRB(1)
.6	.0029	.0020	.0010	.0006
.8	.0028	.0018	.0009	.0006
.9	.0037	.0026	.0013	.0006
.95	.0065	.0049	.0025	.0006
1.05	.0051	.0045	.0022	.0005
1.10	.0047	.0033	.0016	.0008
1.15	.0037	.0027	.0013	.0006
1.25	.0032	.0019	.0009	.0008
1.40	.0027	.0014	.0007	.0008
1.55	.0030	.0019	.0007	.0008
1.80	.0039	.0032	.0009	.0007
2.20	.0037	.0030	.0010	.0006
2.50	.0032	.0024	.0012	.0005

$\pm\Delta C_Y$

	SSLV	ORB	ET	SRB(1)
.6	.0027	.0025	.0005	.0006
.8	.0022	.0020	.0005	.0005
.9	.0017	.0015	.0006	.0004
.95	.0017	.0015	.0007	.0004
1.05	.0018	.0015	.0009	.0004
1.10	.0019	.0015	.0010	.0004
1.15	.0017	.0015	.0007	.0004
1.25	.0017	.0015	.0006	.0004
1.40	.0016	.0014	.0005	.0004
1.55	.0015	.0012	.0006	.0004
1.80	.0015	.0010	.0008	.0005
2.20	.0017	.0008	.0010	.0008
2.50	.0019	.0006	.0012	.0010

Table 8-10

BASE MOMENT INCREMENTS

The general equations for the element moment increments are

$$\Delta C_M = \Delta C_N \left(\frac{X_N}{L}\right) + \Delta C_A \left(\frac{Z_A}{L}\right)$$

$$\Delta C_{YN} = \Delta C_Y \left(\frac{X_{YN}}{L}\right)$$

$$\Delta C_\ell = \Delta C_Y \left(\frac{Z_L}{L}\right) + \Delta C_N \left(\frac{Y_L}{L}\right)$$

The SSLV moment increment is determined by the following equations

$$\Delta C_{M_{SSLV}} = \sqrt{(\Delta C_{M_O})^2 + (\Delta C_{M_{ET}} + \Delta C_{M_{RSRB}} + \Delta C_{M_{LSRB}})^2}$$

$$\Delta C_{YN}_{\ell\,SSLV} = \sqrt{(\Delta C_{YN}_{\ell\,O})^2 + (\Delta C_{YN}_{\ell\,ET})^2 + (\Delta C_{YN}_{\ell\,RSRB})^2 + (\Delta C_{YN}_{\ell\,LSRB})^2}$$

	ORBITER	ET	SRB RIGHT LEFT
$\frac{X_N}{L} =$	.99	.87	1.17
$\frac{Z_A}{L} =$	.31	0.0	0.0
$\frac{X_{YN}}{L} =$	1.06	0.87	0.195
$\frac{Y_L}{L} =$	0.0	0.0	1.17
$\frac{Z_L}{L} =$	.27	0.03	0.0

NOTE; L = 1290 INCHES

Section IX

FOREBODY PLUME INDUCED MATH MODEL

The nominal forebody plume induced aerodynamic characteristics were small except on the Orbiter fuselage, inboard elevon and the vertical tail. Math models were thus developed for the SSLV, Orbiter, the inboard elevon hinge moment and the vertical tail. The SSLV and Orbiter normal force, pitching moment and inboard elevon hinge moment was formulated into the following math model.

$$
C_N = C_{N_{\alpha-\beta \text{ MATRIX}}} + \left[\partial C_N / \partial \delta_{EI_{\substack{\alpha-\beta \\ \text{MATRIX} \\ > \\ <}}} \right] \times \Delta \delta_{EI} + \left[\partial C_N / \partial \delta_{EO_{\substack{> \\ <}}} \right] \times \Delta \delta_{EO_{\substack{\alpha-\beta \\ \text{MATRIX}}}}
$$

$$
C_M =
$$

$$
C_{H_{e_I}} =
$$

where C_N is a 4x7 matrix for $\alpha = +4, 0, -4, -8$
$$\beta = -6, -4, -2, 0, 2, 4, 6$$

elevon deflection corresponds to close schedule 6

$\partial C_N / \partial \delta_{EI_{\substack{> \\ <}}}$ is a 4x7 matrix for $\alpha = +4, 0, -4, -8$
$$\beta = -6, -4, -2, 0, 2, 4, 6$$

> gradient for inboard elevon deflections > nominal

< gradient for inboard elevon deflections < nominal

$\partial C_N / \partial \delta_{EO_{\substack{> \\ <}}}$ is a 4.7 matrix for $\alpha = +4, 0, -4, -8$
$$\beta = -6, -4, -2, 0, 2, 4, 6$$

> gradient for outboard elevon deflections > nominal

< gradient for outboard elevon deflections < nominal

$\Delta \delta_{EI}$ – change in inboard elevon deflection from nominal value to invoard elevon deflection of interest.

$\Delta \delta_{EO}$ – change in outboard elevon deflection from nominal value to outboard elevon deflection of interest.

Typical values of SSLV and Orbiter plume induced forebody normal force coefficients are presented in Table 9-1.

The orbiter normal force and pitching moment math models were derived from the results of the pressure integration of the power-delta pressure coefficients. The orbiter data used to derive the math model is presented in the tabulated date in the Appendix - Section 9 (Forebody Pressure Integration) of the printout sheet (see Section VII). The SSLV and Orbiter math models are identical since only the orbiter plume effects are included in the math model.

The hinge moment math model was derived from the left wing gage data, although the data is presented for the right wing. A comparison of the left wing gage data and the right wing pressure integration data was made to evaluate the best data to use and the gage data had the most consistent trend with changes in attitude and configuration. The left wing gage data used to develop the hinge moment math model is presented in the tabulated data in the appendix in Section 8 (GAGE DATA) of the printout sheet (see Section VII).

The vertical tail shear force, bending moment and torsion moment coefficient were formulated into the following math model

$$C_v = [C_{v_{\alpha-\beta_{Matrix}}}]$$

where

$[C_{v_{\alpha-\beta_{Matrix}}}]$ is a 4 x 7 matrix for $\alpha = +4,0,-4,-8$
$\beta = -6,-4,-2,0,2,4,6$

for elevon deflections noted on the table.

C_{Yv}, vertical tail power delta shear force coefficient

C_{Bv}, vertical tail power delta bending moment coefficient

C_{Tv}, vertical tail power delta torsion moment coefficient

The vertical tail shear force math model includes only the $\alpha-\beta$ matrix at the nominal elevon deflection. No influence of elevon deflections are included. The vertical tail power induced shear force, bending moment, and torsion moment coefficients were developed into table format. A typical example is presented in Table 9-2.

The vertical tail math model was derived from the integration of the vertical tail pressure data presented in the tabulated data in the appendix in Section 9 (Forebody Pressure Integration) of the printout sheet (see Section VII).

FOREBODY COEFFICIENT TOLERANCES

Forebody tolerances have been developed for all forebody elements and components. As mentioned above, only the Orbiter, inboard elevon hinge moment and the vertical tail had measurable plume induced aerodynamic changes that could be effectively modeled. The other elements and components have zero nominal math model plume induced aerodynamic characteristics. Tolerances have been developed for all element and components, however, to account for all possible variations in plume induced aerodynamic characteristics. The forebody element and component force coefficient tolerances are presented as tabled values that are the $\pm 3\sigma$ variation of the nominal coefficient. The $\pm 3\sigma$ variation covers the potential variation of the coefficient from the math model results to expected flight data values.

Examples of the SSLV and element force coefficient tolerances are presented in Table 9-3. The moment increment equations are presented in Table 9-4. Examples of the component force coefficient tolerances and moment equations are presented in Tables 9-5 and 9-6. The moment tolerances require using equations that include the force coefficient tolerances along with the nominal aerodynamic center in conjunction with the nominal forebody power delta (when $\neq 0$) times the aerodynamic center tolerance.

The forebody tolerances include contributions due to 1. test instrumentation uncertainty, 2. simulation parameter uncertainty, 3. Reynolds number characteristics, 4. Model-tunnel testing uncertainties. 5. Pressure integration uncertainties and 6. Math model uncertainties. Each tolerance contribution is assumed independent and therefore the contributions are combined using the RSS technique. The tolerances thus cover the uncertainty from the math model to flight data and are to a $\pm 3\sigma$ level with a Gaussian distribution.

The forebody coefficients are determined using power delta's. Thus the instrumentation accuracy includes two independent measurements that are combined

by the RSS techniques. The instrumentation accuracy for a single measurement
is estimated to be 3 percent. Thus two measurements would be 4.3 percent. The
general uncertainty in the nominal forebody force coefficient due to instrumenta-
tion uncertainty was estimated at 50 percent of the calculated nominal forebody
coefficient. The similarity parameter uncertainty was estimated to be 30 percent
of the nominal, Reynolds number and scale effect was estimated to be 100 percent
of the nominal, model uncertainties were estimated to be 30 percent of the
nominal, integration uncertainties at 30 percent of the nominal and math model
uncertainties were estimated at 20 percent of the nominal value. The net RSS
tolerance value for the forebody coefficients are large compared to the nominal
math model values. This is because the nominal math model force coefficients
are small. If the math model is not used the tolerance would be approximately
double the values presented and it was determined that forebody tolerances
approach double the values would be excessive.

Portions of the forebody have zero nominal plume induced aerodynamic force
coefficients in the math model although specific computed values have been
determined and are listed in the tabulated data in the appendix (see Section
VII). The tolerance analysis discussed above considered the nominal values
calculated although the math model nominal force coefficients are zero.

Table 9-1. SSLV AND ORBITER POWER DELTA - NORMAL FORCE COEFFICIENT - FOREBODY

MACH	δe_{IO}	α	β						
			-6	-4	-2	0	+2	+4	+6
1.10	10/9	4	+.0063	+.0061	+.0058	+.0056	+.0058	+.0061	+.0063
		0	+.0085	+.0080	+.0070	+.0053	+.0070	+.0080	+.0085
		-4	+.0090	+.0085	+.0080	+.0075	+.0080	+.0085	+.0090
		-8	+.0096	+.0093	+.0090	+.0088	+.0090	+.0093	+.0096
1.15	10/5	4	+.0080	+.0077	+.0057	+.0053	+.0057	+.0077	+.0080
		0	+.0079	+.0075	+.0057	+.0052	+.0057	+.0075	+.0079
		-4	+.0080	+.0077	+.0072	+.0070	+.0072	+.0077	+.0080
		-8	+.0095	+.0092	+.0081	+.0075	+.0081	+.0092	+.0095
1.25	10/-2	4	+.0043	+.0048	+.0053	+.0058	+.0053	+.0048	+.0043
		0	+.0055	+.0059	+.0063	+.0067	+.0063	+.0059	+.0055
		-4	+.0070	+.0070	+.0071	+.0071	+.0071	+.0070	+.0070
		-8	+.0093	+.0096	+.0099	+.0102	+.0099	+.0096	+.0093
1.40	10/-2	4	+.0060	+.0056	+.0051	+.0047	+.0051	+.0056	0.0060
		0	+.0060	+.0056	+.0051	+.0047	+.0051	+.0056	+.0060
		-4	+.0068	+.0070	+.0073	+.0075	+.0073	+.0070	+.0068
		-8	+.0096	+.0101	+.0105	+.0108	+.0105	+.0101	+.0096

Table 9-2. VERTICAL TAIL SIDE FORCE POWER DELTA

MACH	$\delta_{e_{IO}}$	α	β -6	-4	-2	0	+2	+4	+6
.6	10/9	4	+.0339	+.0226	+.0113	+.0000	-.0113	-.0226	-.0339
		0	+.0278	+.0185	+.0093	+.0000	-.0093	-.0185	-.0278
		-4	+.0302	+.0201	+.0100	+.0000	-.0100	-.0201	-.0302
		-8	+.0249	+.0166	+.0083	+.0000	-.0083	-.0166	-.0249
.8	10/9	4	+.0129	+.0086	+.0043	+.0000	-.0043	-.0086	-.0129
		0	+.0080	+.0053	+.0026	+.0000	-.0026	-.0053	-.0080
		-4	+.0014	+.0010	+.0005	+.0000	-.0005	-.0010	-.0014
		-8	+.0015	+.0010	+.0005	+.0000	-.0005	-.0010	-.0015
.9	10/9	4	+.0170	+.0113	+.0057	+.0000	-.0057	-.0113	-.0170
		0	+.0170	+.0113	+.0057	+.0000	-.0057	-.0113	-.0170
		-4	+.0210	+.0140	+.0070	+.0000	-.0070	-.0140	-.0210
		-8	+.0158	+.0105	+.0053	+.0000	-.0053	-.0105	-.0158
.95	10/9	4	+.0689	+.0459	+.0230	+.0000	-.0230	-.0459	-.0689
		0	+.0654	+.0436	+.0218	+.0000	-.0218	-.0436	-.0654
		-4	+.0615	+.0410	+.0205	+.0000	-.0205	-.0410	-.0615
		-8	+.0566	+.0377	+.0188	+.0000	-.0188	-.0377	-.0566
1.05	10/9	4	+.0369	+.0246	+.0123	+.0000	-.0123	-.0246	-.0369
		0	+.0340	+.0227	+.0113	+.0000	-.0113	-.0227	-.0340
		-4	+.0279	+.0186	+.0093	+.0000	-.0093	-.0186	-.0279
		-8	+.0315	+.0210	+.0105	+.0000	-.0105	-.0210	-.0315

Table 9-3

FOREBODY FORCE COEFFICIENT TOLERANCES - SSLV AND ELEMENTS

$\pm\Delta C_A$

MACH NO.	SSLV	ORB	ET	SRB(1)
.6	.0038	.0010	.0010	.0025
.8	.0038	.0010	.0010	.0025
.9	.0038	.0010	.0010	.0025
.95	.0052	.0012	.0012	.0035
1.05	.0037	.0017	.0017	.0020
1.1	.0035	.0015	.0015	.0020
1.15	.0035	.0015	.0015	.0020
1.25	.0045	.0014	.0014	.0025
1.40	.0040	.0013	.0013	.0025

$\pm\Delta C_N$

.6	.0068	.0060	.0030	.0010
.8	.0077	.0070	.0030	.0010
.9	.0094	.0080	.0040	.0020
.95	.0101	.0080	.0050	.0025
1.05	.0099	.0080	.0055	.0015
1.1	.0089	.0070	.0050	.0015
1.15	.0067	.0050	.0040	.0015
1.25	.0055	.0030	.0030	.0025
1.40	.0079	.0030	.0020	.0050

$\pm\Delta C_Y$

.6	.0083	.0080	.0005	.0015
.8	.0083	.0080	.0005	.0015
.9	.0093	.0090	.0006	.0015
.95	.0109	.0100	.0007	.0030
1.05	.0098	.0080	.0010	.0040
1.10	.0093	.0060	.0010	.0050
1.15	.0082	.0040	.0008	.0050
1.25	.0064	.0030	.0006	.0040
1.40	.0052	.0030	.0006	.0030

Table 9-4

FOREBODY MOMENT INCREMENT EQUATIONS - SSLV AND ELEMENTS

ELEMENTS

$$\Delta C_M = \sqrt{\left[\Delta C_N \left(\frac{X_N}{L}\right)\right]^2 + \left[C_N \left(\frac{\Delta X_N}{L}\right)\right]^2 + \left[\Delta C_A \left(\frac{Z_A}{L}\right)\right]^2}$$

$$\Delta C_{YN} = \sqrt{\left[\Delta C_Y \left(\frac{X_{YN}}{L}\right)\right]^2 + \left[\Delta C_A \left(\frac{Y_{ZL}}{L}\right)\right]^2}$$

$$\Delta C_\ell = \sqrt{\left[\Delta C_Y \left(\frac{Z_L}{L}\right)\right]^2 + \left[\Delta C_N \left(\frac{Y_L}{L}\right)\right]^2}$$

SSLV TYPICAL

$$\Delta C_{M_{SSLV}} = \sqrt{(\Delta C_{M_O})^2 + (\Delta C_{M_{ET}})^2 + (\Delta C_{M_{RSRB}})^2 + (\Delta C_{M_{LSRB}})^2}$$

MACH	ORB $\frac{X_N}{L}$	$\frac{\Delta X_N}{L}$	$\frac{X_{YN}}{L}$	$\frac{Z_L}{L}$	$\frac{Y_{ZL}}{L}$	$\frac{Y_L}{L}$	$\frac{Z_A}{L}$	ET $\frac{X_N}{L}$	$\frac{\Delta X_N}{L}$	$\frac{X_{YN}}{L}$	$\frac{Z_L}{L}$	$\frac{Y_{ZL}}{L}$	$\frac{Y_L}{L}$	$\frac{Z_A}{L}$
.6	.92	.03	.98	.42	0	0	.26	.7	0	.7	.03	.03	.03	.03
.8	.93	.03	.94	.42	0	0	.26	.7	0	.7	.03	.03	.03	.03
.9	.96	.03	1.02	.43	0	0	.26	.8	0	.8	.03	.03	.03	.03
.95	1.01	.03	1.03	.44	0	0	.26	.8	0	.8	.03	.03	.03	.03
1.05	.95	.04	1.02	.45	0	0	.26	.8	0	.8	.03	.03	.03	.03
1.10	.96	.03	1.01	.45	0	0	.26	.8	0	.8	.03	.03	.03	.03
1.15	.97	.02	1.0	.44	0	0	.26	.8	0	.8	.03	.03	.03	.03
1.25	.98	.02	1.0	.44	0	0	.26	.8	0	.8	.03	.03	.03	.03
1.40	.99	.02	1.0	.44	0	0	.26	.8	0	.8	.03	.03	.03	.03

SRB RIGHT LEFT

MACH	$\frac{X_N}{L}$	$\frac{\Delta X_N}{L}$	$\frac{X_{YN}}{L}$	$\frac{Z_L}{L}$	$\frac{Y_{ZL}}{L}$	$\frac{Y_L}{L}$	$\frac{Z_A}{L}$
.6	1.15	0	1.15	0	.194	.194	.02
.8	1.15	0	1.15	0	.194	.194	.02
.9	1.15	0	1.15	0	.194	.194	.02
.95	1.14	0	1.14	0	.194	.194	.02
1.05	1.14	0	1.14	0	.194	.194	.02
1.10	1.13	0	1.13	0	.194	.194	.02
1.15	1.10	0	1.10	0	.194	.194	.02
1.25	1.10	0	1.10	0	.194	.194	.02
1.40	1.10	0	1.10	0	.194	.194	.02

NOTE: L = 1290 INCHES

Table 9-5

FOREBODY FORCE TOLERANCES — COMPONENTS

WING TOLERANCES		VERTICAL TAIL TOLERANCES
MACH	$\pm\Delta CNW$	$\pm\Delta CYV$
.6	.0050	.010
.8	.0050	.010
.9	.0050	.030
.95	.0050	.030
1.05	.0060	.030
1.10	.0065	.010
1.15	.0060	.008
1.25	.0040	.010
1.40	.0040	.006

Table 9-6

FOREBODY MOMENT EQUATIONS — COMPONENTS

WING

$$\Delta C_{BW} = \Delta C_{NW} \left(\frac{y_w}{b}\right)$$

$$\Delta C_{TW} = \Delta C_{NW} \left(\frac{x_w}{\bar{c}}\right)$$

VERTICAL TAIL

$$\Delta C_{BV} = \sqrt{\left[\Delta C_{YV} \left(\frac{Z_V}{L}\right)\right]^2 + \left[C_{YV} \left(\frac{\Delta Z_V}{L}\right)\right]^2}$$

$$\Delta C_{TV} = \sqrt{\left[\Delta C_{YV} \left(\frac{X_V}{L}\right)\right]^2 + \left[C_{YV} \left(\frac{\Delta X_V}{L}\right)\right]^2}$$

HINGE MOMENT

$$\Delta CHEI = \Delta CHEI$$

$$\Delta CHEO = \Delta CHEO$$

| MACH | WING [1] | | VERTICAL [2] | | | | | |
	$\frac{y_w}{b}$	$\frac{x_w}{\bar{c}}$	$\frac{Z_V}{L}$	$\frac{\Delta Z_V}{L}$	$\frac{X_V}{L}$	$\frac{\Delta X_V}{L}$	$+\Delta CHEI$	$+\Delta CHEO$
.6	.091	-.22	.60	.20	.34	.10	.0050	.0020
.8	.095	-.20	.75	.20	.33	.10	.0050	.0015
.9	.098	-.27	.42	.20	.59	.17	.0100	.0040
.95	.105	-.26	1.10	.25	.84	.20	.0130	.0100
1.05	.110	-.26	.72	.30	.51	.25	.0100	.0030
1.10	.100	-.28	.91	.30	.81	.20	.0080	.0010
1.15	.110	-.32	.63	.20	.87	.20	.0070	.0010
1.25	.110	-.33	.34	.15	.78	.15	.0050	.0010
1.40	.110	-.32	.45	.30	.40	.10	.0050	.0010

1 *For Wing*

  $b = 936.68''$
  $c = 474.81''$

2 *Vertical*

  $L = 199.8 \ in.$

Section X

CONCLUSIONS

The data from tests IA119 and IA138 resulted in an appreciable amount of good plume induced aerodynamic data. Problems with the data were very limited and the power off data compares very good with other tests.

The major independent variables that change the plume induced aerodynamic characteristics are angle of attack, angle of sideslip, inboard elevon deflection and SRB and SSME power level. Plume induced aerodynamic characteristics and their tolerances for the base and forebody have been developed into math models compatible with the forebody math models.

A math model of the plume induced aerodynamic coefficients for the base was developed for the Mach number range from 0.6 to 2.5. Data tables of these coefficients have been provided in G.E. mass format for computer simulation. A math model of the forces and moments for the base was also developed covering the portion of ascent flight up to 160,000 ft. The data tables for the base force math model was also provided in G.E. mass format. A math model of the forebody plume induced aerodynamic coefficients was also developed and the data tables provided in G.E. mass format. The tolerances for the plume induced aerodynamic coefficients and the tolerance math models for the base and forebody were developed and data tables provided in G.E. mass format.

The plume induced aerodynamic characteristics of the orbiter base are the result of a complicated integration of pressure coefficients and power delta pressure coefficients. These aerodynamic characteristics were developed such that when combined with the forebody data they produce the proper total vehicle aerodynamic characteristics.

The ET base plume induced axial force is larger than previous analyses have predicted, however, it is felt that the present results are consistent and representative of the ET base pressure environment.

The plume induced near field (base environment) and far field (orbiter forebody wing and hinge moment data) had good consistent trends when plotted versus the plume similarity parameter. The consistency of the data for both the near field and far field added confidence in the similarity parameter used.

Section XI

RECOMMENDATIONS

A computer program was developed to integrate the pressure data for all elements and components and tabulate the results and the results of the gage data. The tabulated results and plotted power variation data represent approximately 2000 computer printout pages. Time did not permit an extensive analysis of all the data. It is recommended that additional analyses be conducted of the vertical tail data, wing data, inboard hinge moment data and orbiter fuselage data.

It is also recommended that the IA119 and IA138 test results be reevaluated using the new similarity parameters.

Section XII

REFERENCES

1. Boyle, W. W. and Conine, B. H., "Space Shuttle Plume Simulation/Application - Final Report Results and Math Model, NSI Report TR-230-1962, dated 15 July 1978.

2. Boyle, W. W., Conine, B. H., and Bell, G., "Space Shuttle Plume Simulation/ Application — Final Report Results and Math Model — Supersonic Data", NSI Report TR-230-1963, dated 15 May 1979.

3. Dziubala, T. J. and Marroquin, J., "Pretest Information for Test IA119 of the 0.020-Scale 88-OTS Configuration 140 C (Modified) Integrated Space Shuttle Vehicle Test-Plume Model in the NASA/ARC UP WT 11 by 11 Foot Leg for Determination of Aspiration-Induced Effects", Document SD-77-SH-0196, Rockwell International, Space Division, September 20, 1977.

4. Marroquin, J., "Pretest Information for Test IA138 of the 0.010-Scale 75-OTS Jet Plume Space Shuttle Model in the 9x7-Foot Leg of the NASA/ARC Unitary Plan Wind Tunnel", Document SD78-SH-0133, Rockwell International, Space Division, 12 June 1978.

5. Harden, R. B. and Campbell, J. R. II, "Pretest Information for Test IA19 of the 0.02 Scale 88-OTS Jet Plume Space Shuttle Model in the 11x11 Foot Leg of the NASA/ARC Unitary Plan Wind Tunnel", Document 5074-SH-0276, Rockwell International Space Division, dated 9 March 1974.

6. Andrews, C. D., "MSFC Input for RI/SD SSLV Wind Tunnel Tests IA119/IA138 NASA Memo ED32-77-13, dated 23 February 1977.

7. Boyle, W. W., "Plume Technology Program Base Pressure Similarity Parameters", NSI Memo M-9230-76-45, dated July 1976.

8. Sims, Joseph L., "Plume Simulation Technology", MSFC Systems Dynamics Laboratory Viewgraph Presentation, January 1979.